WING/BODY INTERFERENCE FOR SWEPTBACK WINGS WITH SPECIAL REFERENCE TO PITCHING MOMENT

By. M. Gordon Smith.

SUMMARY.

The object of this paper is to investigate the effect of wing/body interference on the aerodynamic centre position of a family of wing/body combinations.

The combinations cover a range of aspect ratios from 2 to 5 and angles of sweepback from 0° to 60°. Of the two bodies tested one is of variable length and the ratio of body diameter to wing span varies from 0.1 to 0.4. The tests have been performed in a low speed wind tunnel at a Reynolds Number of 0.27×10^{6}, based on wing chord.

In addition, a theoretical analysis covering the wing/body combinations used in the experimental work is described. The method is based on that published by Schlichting but a number of modifications have been made. The most important of these is that the spanwise lift distribution is calculated for each wing and wing/body combination instead of just for the unswept wing. The volume of work involved necessitated the use of a DEUCE computer.

The experimental results are compared with those from two other sources and the results of the theoretical

analysis. The comparison with the purely experimental results shows the same trends in the variation of $\left(-\frac{\Delta K_n}{\bar{c}}\right)$ once account has been taken of the differences between the configurations of the wing/body combinations. Comparison with the theoretical results reveals that the theory predicts the experimental curves quite well, indicating that the modifications are beneficial to the accuracy of the results.

Although no quantitative generalisations can be made it may be said that at low angles of sweepback an increase in sweepback produces a decrease in the forward movement of the aerodynamic centre due to a body. At high angles of sweepback each combination must be treated individually. The combinations in this paper tend to produce an increase in the forward movement of the aerodynamic centre at the higher angles of sweepback.

WING/BODY INTERFERENCE FOR SWEPTBACK WINGS WITH SPECIAL REFERENCE TO PITCHING MOMENT

by

M. Gordon Smith. B.Sc.

Department of Aeronautics,

University of Glasgow.

January 1964

This paper has been submitted as a thesis for the Degree of M.Sc. at the University of Glasgow. The author would like to acknowledge the assistance and encouragement given by Professor T.R.F. Nonweiler and Doctor A.W. Babister, and would like to thank the workshop and wind tunnel staffs without whose help the experimental work could not have been performed. The assistance of the staff of the Computing Department is also gratefully acknowledged.

WING/BODY INTERFERENCE FOR SWEPTBACK WINGS WITH SPECIAL REFERENCE TO PITCHING MOMENT

SUMMARY.

The object of this paper is to investigate the effect of wing/body interference on the aerodynamic centre position of a family of wing/body combinations.

The combinations cover a range of aspect ratios from 2 to 5 and angles of sweepback from 0° to 60°. Of the two bodies tested one is of variable length and the ratio of body diameter to wing span varies from 0.1 to 0.4. The tests have been performed in a low speed wind tunnel at a Reynolds Number of 0.27×10^{6}, based on wing chord.

In addition, a theoretical analysis covering the wing/body combinations used in the experimental work is described. The method is based on that published by Schlichting but a number of modifications have been made. The most important of these is that the spanwise lift distribution is calculated for each wing and wing/body combination instead of just for the unswept wing. The volume of work involved necessitated the use of a DEUCE computer.

The experimental results are compared with those from two other sources and the results of the theoretical

analysis. The comparison with the purely experimental results shows the same trends in the variation of $\left(-\frac{\Delta K_n}{\bar{c}}\right)$ once account has been taken of the differences between the configurations of the wing/body combinations. Comparison with the theoretical results reveals that the theory predicts the experimental curves quite well, indicating that the modifications are beneficial to the accuracy of the results.

Although no quantitative generalisations can be made it may be said that at low angles of sweepback an increase in sweepback produces a decrease in the forward movement of the aerodynamic centre due to a body. At high angles of sweepback each combination must be treated individually. The combinations in this paper tend to produce an increase in the forward movement of the aerodynamic centre at the higher angles of sweepback.

CONTENTS.

SYMBOLS.

A	Aspect ratio $= \frac{b^2}{S}$.
b	Wing span.
C	Wing root chord.
c	Wing chord.
$\bar{c}$	Geometric mean wing chord.
$\bar{\bar{c}}$	Aerodynamic mean wing chord.
C_L	Total Lift coefficient.
C_D	Drag coefficient.
C_M	Pitching moment coefficient.
c_l	Local Lift coefficient.
$\frac{dC_L}{d\alpha}$	Lift curve slope.
$\frac{dC_M}{dC_L}$	Slope of C_M vs. C_L curve.
$\left(\Delta\frac{dC_M}{dC_L}\right)$	Change in $\frac{dC_M}{dC_L}$ due to the influence of the body. $= \left(-\frac{\Delta K_n}{\bar{\bar{c}}}\right)$
$\frac{e}{l_b}$	Non-dimensional body nose length based on axis of symmetry quarter chord point.
$\left(-\frac{\Delta K_n}{\bar{\bar{c}}}\right)$	Forward movement of the aerodynamic centre.
L_B, l_b	Body length.
$\frac{L_N}{L_B}$	Non-dimensional body nose length based on root quarter chord point.
$\frac{M}{C}$	Non-dimensiomal body nose length based on wing root leading edge.

$\frac{N}{C}$	Non-dimensional body tail length based on wing root trailing edge.
q	Dynamic pressure.
R.N.	Reynolds Number.
S	Total wing area.
s	Wing semi-span.
x, y, z	Cartesian co-ordinates.
$\frac{d\varepsilon}{d\alpha}$	Rate of downwash with incidence.
η	Non-dimensional spanwise unit, $= \frac{2y}{b}$.
$\overline{x}, \overline{y}$	Co-ordinates of semi-span aerodynamic centre.
$\frac{x}{c}$	Non-dimensional longitudinal co-ordinate, for downwash distribution.

Suffices.

W	Wing.
B	Body.
BW	Wing/body combination.

1. INTRODUCTION.

1.1 As has been observed by various people [1,2,3] in their summaries of the situation regarding wing/body combinations and the mutual interference effects present, the prediction of the aerodynamic forces and moments produced in such combinations is much more involved than the pure algebraic addition of the forces and moments experienced by the individual components. In many cases the interference effects are of the same order of magnitude as the forces and moments of the individual components and thus their investigation becomes of great importance.

In his paper, Blair [3] considered the effect of a body on the spanwise lift distribution and on the lift curve slope. There will be an attempt in this paper to extend this work to the consideration of the shift of the aerodynamic centre due to the body using swept back wings. This work has already been done by Schlichting [11], but since the publication of his results improvements have been made in the methods that he employed. These will be incorporated in the present paper.

When considering sweptback wing/body combinations there are three criteria which may be observed as the angle of sweepback is increased. These are as follows, keeping (1) the axis of symmetry chord, (2) the mean aerodynamic

chord, (3) the root chord in a constant longitudinal position. The first two cases have been covered in Reference (11) while the third is considered in this paper.

The series of wind tunnel tests which is described in the next section was performed to find the magnitude of this effect and its dependence on the parameters of the wing body combination. The tests covered the combination of a family of swept wings with a family of bodies. The combinations represented very approximately the configurations in present day use.

The accent in this paper will be on the physical interpretation of the results and a comparison of them, as far as is possible, with the results published by other investigators and with those obtained by theory.

From references (4) and (5) one can obtain results for the shift of the aerodynamic centre due to the addition of a body on an unswept wing by empirical formulae and charts. No such equivalent appears to exist for swept wings. But it is hoped that this paper may give some indication of the trends to be expected in the shift of the aerodynamic centre with variation in the major parameters of the wing/body combination and the extent to which these may be forecast by the application of suitable theory.

1.2 In Section 2 the experimental work will be described, giving details of the wind tunnel models and the range covered by the tests, mentioning the form of presentation of the results. Following this, the next section deals with the various theories available for the treatment of this subject and gives a description of the method which appears most versatile and practical for the handling of as wide a range of configurations as possible with a fair degree of accuracy. In Section 4 the experimental results are discussed and compared with those of other reports and with theoretical results. The conclusions are drawn in the next section. Sections 6 onwards give the results in tabular and graphical form and a brief description of the numerical procedure followed in the theoretical work.

2. EXPERIMENTAL CONSIDERATIONS.

2.1 A series of more than 200 wind tunnel tests were performed in a low speed wind tunnel having a working section of dimensions 2.75 feet x 3.75 feet in which the normal wind velocity was 85 ft./sec. The Reynolds Number at this velocity, based on the wing chord, was 0.27×10^6. The Turbulence Factor of the Tunnel, as obtained by a Turbulence Sphere [6], was 1.65. The tunnel was equipped with a three component balance.

The models, being of the same type as those used by Blair [3], were machined from aluminium. The family of wings consisted in three unswept, untapered wings of aspect ratios 2, 3 and 4, and twelve swept, untapered wings of aspect ratios 2, 3, 4 and 5. The angles of sweepback covered were 30°, 45° and 60°. The aspect ratio change was effected by adding or removing detachable sections having joints of such a type as to make them completely interchangable. Care was taken to ensure positive sealing of the joints.

It is important to note that all the wings had the same aerofoil section in a streamwise direction - N.A.C.A. 0012, and all had the same streamwise chord of 6 inches with straight tips.

The family of bodies consisted in two circular

cylindrical bodies with semi—elliptical noses and conical tails, having maximum diameters of 3 inches and 4.5 inches, and lengths of 27.5 inches and 41.25 inches respectively. The 3 inch diameter body had detachable sections which allowed 5 different body lengths and 4 longitudinal wing positions. All tests were carried out with a mid—wing configuration, the wing having no incidence relative to the body longitudinal axis. The bodies were also tested on their own. Table (1) gives the range of configurations covered in greater detail, while Figure (1) shows a typical wing and wing/body combination.

2.2 The wing/body combinations were mounted with a single supporting strut, the hinge point being at the quarter chord point of the root chord. For testing the wings alone the hinge point was on, or a little behind, the quarter chord point of the wing chord at the axis of symmetry. Bodies alone were tested with the hinge point at the same position as in the combinations, the wings being replaced by a short centre section which did not protrude beyond the body wall. The incidence change was produced by altering the length of the adjustable tail strut.

Some tests were performed with images [6] of the support system projecting from the roof of the tunnel to

investigate the effect of the support system on the measurements.

Further to the main series of tests some flow visualization tests were carried out, using tufts, to give a clearer picture of the flow, especially at high angles of sweepback. Some doubt existed as to the assumptions that could be made when considering the theoretical analysis. It was hoped that the flow visualization tests would help in this, the main points that were studied being the point of separation on the rear of the body, the flow at the wing/body junction and tip, and the flow at the centre section of the swept back wings when tested on their own.

Since the accuracy of the measurement of the pitching moment was of extreme importance great care was taken to ensure that the hinge points in the main and tail struts were as free as possible without being excessively so. This was done by accurate machining and careful assembly of the models. However, as a further precaution, each test was repeated and the mean results used. In some cases where doubt still remained, especially with the unswept wings where the change in the pitching moment with incidence was small, the tests were repeated two or three times to obtain a reliable result.

2.3 The Lift, Drag and Pitching Moment were

measured in the range of incidence from -8° to $+20^{\circ}$. The values of the three coefficients were calculated and then referred to the quarter chord point of the mean aerodynamic chord. This point was chosen since it is the most common reference point when quoting wind tunnel results. It may be noted in passing that it can be proved very simply that the shift of the aerodynamic centre due to a body is independent of the point of reference. Because of the large amount of data to be processed the work was done on a DEUCE computer using a very simple programme, a broad outline of which appears in Appendix (1).

C_L was plotted against incidence and C_M was plotted against C_L. The values were uncorrected for wind tunnel interference on the grounds of the conclusion of Reference (7) that the interference had negligible effect on the pitching moment. A representative selection of the graphs obtained appears in Figures (2) to (5). Since only the slope of the C_M against C_L curve is required, a full reproduction of the curves is unneccesary. Table (2) and (3) contain all the values that were obtained of $\frac{dC_M}{dC_L}$ and $\left(\Delta\frac{dC_M}{dC_L}\right)$ due to the body respectively.

Figures (6) to (9) show the variation of the shift of the aerodynamic centre due to the influence of

the body with change in aspect ratio and sweepback, body nose and tail length and body diameter. All the parameters are quoted non-dimensionally. Again only a representative selection of the curves has been given when the trend shown appears to be nearly independent of that particular variable.

It should be noted that the body nose and tail lengths are measured from the wing root leading and trailing edges respectively. Apart from the fact that this method is used in Reference (4) the models are constructed in such a way that a change in the angle of sweepback does not alter the longitudinal position of the wing root chord.

In Figures (10) to (14) will be found results of $\left(\Delta\frac{dC_M}{dC_L}\right)$ due to a body from References (4),(5),(8),(9), (10) and (11). Sketches of the flow patterns observed in the tuft tests appear in Figure (19). These are confined to the flow observed at low incidence.

3. THEORETICAL CONSIDERATIONS.

3.1 In this paper the object of the theoretical work is to try to predict the actual shift of the aerodynamic centre due to a body for the configurations employed in the wind tunnel tests. At present only References (4) and (5) give a quick means of predicting this shift and these are only valid for unswept wings. There appears to be no such equivalent for swept wings.

The shift of the aerodynamic centre due to the effect of a body can be divided into two parts, (a) the stabilising nose-down moment due to the loss of lift over the centre section of the wing and (b) the destabilising nose-up moment due to the lift acting on the body.

It is the sum of these two moments which decides the direction and magnitude of the resultant shift. Both moments are dependent on the angle of sweepback. In general, the forward movement of the aerodynamic centre due to the body should decrease as angle of sweepback is increased [11].

The two moments are considered separately in the next sections.

3.2 To calculate the contribution of the wing to the shift of the aerodynamic centre it is necessary to obtain

the change in the spanwise lift distribution brought about by the body. Much work has been done on this subject and there are various methods available. These have already been fully examined and compared in References (2) and (3) in which will be found a complete bibliography. In Reference (3), Blair compared several theories with the view to finding the most versatile one for the handling of as wide a range as possible. The conclusion reached by Blair was that the method of Muthopp [12] was the most useful. In its basic form this theory can be applied only to unswept wings but it has since been extended [13] to cover the effect of sweepback, finite wing thickness and large root chords compared with body diameter.

The unmodified form of Multhopp's method has been used in References (4),(5) and (11), where the shift of the aerodynamic centre due to the effect of a body was considered. Reference (2) makes the comment that it would appear that Multhopp's method was quite suited to the prediction of this shift since the results obtained agreed well with experimental results.

It should be noted that the most accurate spanwise and chordwise lift distribution of a wing alone would be obtained from a lifting surface theory but the application of such a theory to wing/body combinations

would be very much more complicated. In view of the accuracy in the prediction of the shift of the aerodynamic centre that can be obtained using lifting line methods further refinement but at the cost of considerable complication would be unneccesary for the purposes of this paper.

3.21 The method of calculation to obtain the shift of the aerodynamic centre due to loss of wing lift will follow the general lines laid down in Reference (11). In this reference Schlichting made use of Multhopp's lifting line theory as it stood at that time [14], allowing a diminution in sectional lift curve slope from the two-dimensional value on the exposed wing to one-third of that value over the portion of the wing covered by the body. The local aerodynamic centre was assumed to lie always on the quarter chord line. The shift in the aerodynamic centre due to loss of wing lift was calculated for the unswept wing only, the effect of sweepback being considered purely as a change in moment arm measured from the mean quarter chord point. This simplification was based on the assumption that since only the difference in lift distribution was being considered the errors involved would disappear to a first approximation.

The method to be used here is that of Multhopp [12], extended as in Reference (13). This method is fully discussed in References (3) and (13) so there is no need to

do so here. The effect of the body on the spanwise lift distribution will be calculated for each angle of sweepback. The shift in the aerodynamic centre will be calculated assuming that the local aerodynamic centre lies on the quarter chord line except near the centre section or the wing/body junction where there is a backward movement and near the tip where the movement is forward [15].

At the wing/body junction the body wall has a reflecting effect and the conditions that exist here are assumed to be similar to those that exist at the axis of symmetry of a wing alone. Thus, at the wing/body junction the displacement of the local aerodynamic centre from the quarter chord line is taken to be equal to its displacement at the axis of symmetry of the wing alone and the locus across the body is a straight line at right angles to the body longitudinal axis.

Having obtained the spanwise lift distribution for both the wing alone and the wing/body combination it is possible to calculate the pitching moments through the mean quarter chord point, see Figure (1). The pitching moment due to the lift acting on a strip at a distance (y) from the axis of symmetry, with its quarter chord point at a distance (x) from the lateral axis through the mean quarter chord point, and the local displacement of the

aerodynamic centre from the quarter chord line of the wing being $\Delta(h_y)$, is

$$dM = (x - \Delta h_y).dL$$

$$= \left[(\bar{y} - y).\tan\varphi - \Delta h_y\right].dL$$

Also, $dL = q.c_{l_y}.c_y.dy$, and hence

$$dM = q.c_{l_y}.\left[(\bar{y} - y).\tan\varphi - \Delta h_y\right].c_y.dy.$$

Therefore the pitching moment of the wing alone is

$$M_W = 2.q.\int_{y=0}^{\frac{b}{2}} \left\{c_{l_y}.\left[(\bar{y} - y).\tan\varphi - \Delta h_y\right]\right\}_W.c_y.dy \quad .. \quad (1)$$

and that of the wing/body combination is

$$M_{BW} = 2.q.\int_{y=0}^{\frac{b}{2}} \left\{c_{l_y}.\left[(\bar{y} - y).\tan\varphi - \Delta h_y\right]\right\}_{BW}.c_y.dy \quad ..(2)$$

The difference between the two moments is

$$\Delta M = M_{BW} - M_W \quad . \quad . \quad . \quad . \quad . \quad . \quad . \quad . \quad . \quad . \quad . \quad . \quad . \quad . \quad . \quad . \quad . \quad . \quad . \quad (3)$$

and the forward movement of the aerodynamic centre $\left(-\Delta K_n\right)$ due to the loss of wing lift can be obtained from the equation

$$\Delta M = \left(-\Delta K_n\right).L_W \quad . \quad . \quad . \quad . \quad . \quad . \quad . \quad . \quad . \quad . \quad . \quad . \quad . \quad . \quad . \quad . \quad . \quad . \quad . \quad (4)$$

where $L_W = C_{LW}.q.S$ is the lift of the wing alone.

From equations (1),(2),(3) and (4) and making

the parameters non-dimensional

$$\left(-\frac{\Delta K_n}{\bar{\bar{c}}}\right) = \frac{A}{2}\cdot\frac{1}{\frac{dC_{L_W}}{d\alpha}}\cdot\int_{\eta=0}^{1}\left\{\left\{c_{l\eta}\cdot\left[(\bar{\eta}-\eta).\tan\varphi - \Delta h_\eta\right]\right\}_{BW} - \left\{c_{l\eta}\cdot\left[(\bar{\eta}-\eta).\tan\varphi - \Delta h_\eta\right]\right\}_{W}\right\}\cdot\frac{c_\eta}{\bar{\bar{c}}}\cdot d\eta \quad . \quad . \quad . \quad (5)$$

This integral can be evaluated when the spanwise lift distributions and the displacements of the local aerodynamic centre are known. Table (4) shows the results of this calculation for several of the wing/body combinations used in the experimental tests. Table (4) gives the values of $\frac{dC_L}{d\alpha}$ obtained. It should be noted that the shift of the aerodynamic centre as obtained from equation (5) depends mainly on the wing plan form and the ratio of body diameter to wing span and not on the longitudinal position of the wing on the body.

One important difference between equation (5) and the corresponding equation in Reference (11) is that here the value of $\frac{dC_L}{d\alpha}W$ varies with the angle of sweepback while in Reference (11) the value is constant.

3.3 The moment experienced by the body is produced by a certain distribution of lift which can be divided into three parts, (1) the positive lift on the nose and the equal negative lift on the tail of the isolated body, (2) the lift produced by the downwash distribution associated with the

bound and trailing vortices of the wing, and (3) the lift caused by the vertical component of the skin friction forces.

The first two lift distributions have been combined by Multhopp [12] into an expression based on that given by Munk [16]. The third contribution to the moment on the body is a function of the square of the incidence and may be neglected at low values of incidence. In addition there are the moments produced by the normal forces [2] at the nose and tail and the additional lift produced at the tail by the closure of the streamlines [2]. These effects are small at low angles of incidence and may be neglected also.

In order to approach as closely as possible to the physical situation as it occurs in the wind tunnel tests, it is neccesary to make some assumption concerning the state of the flow at the rear of the body. At the low Reynolds Number being employed in the tests it could be assumed as a first approximation that the flow would separate from the body at the junction of the cylindrical centre section of the body and the conical tail. But in the course of the tuft tests it was observed that the flow over the rear of the body, aft of a point just behind the wing root trailing edge, was disturbed by the presence of the main support wind shield. In consequence the prediction of

the point at which the flow breaks away at the rear of the body is made very difficult. In order to cover every possibility the moment on the body will be calculated for the case in which the flow does not break–away at all and, in addition, for the case where break–away occurs at the wing root trailing edge. The actual point of break–away of the flow will occur somewhere between these two extremes.

3.31 The moment experienced by the body is a pure moment and is therefore independent of the axis to which it is referred.

The moment can be calculated from the expression given by Multhopp[12]

$$\frac{1}{q}.\frac{dM_B}{d\alpha} = \frac{\pi}{2}.\int_{x=-l_t}^{l_n} b_B^2(x).\frac{d\beta}{d\alpha}.dx \quad \ldots\ldots\ldots\ldots (6)$$

where (x) is measured from the origin which is situated at the junction of the axis of symmetry and the quarter chord line produced into the body from the wing root. (l_n) and (l_t) are the lengths of the body nose and tail respectively, measured from the origin, and $b_B(x)$ is the local diameter of the body and (β) is the effective angle of incidence of the body.

The movement of the aerodynamic centre due to the moment on the body is

$$\left(-\Delta K_n\right)^1 = \frac{1}{L_W}.M_B \quad \ldots\ldots\ldots\ldots\ldots\ldots\ldots (7)$$

where, $L_W = C_{L_W} . q . S$ . . . . . (8)

Introducing non-dimensional quantities as before

$$\left(-\frac{\Delta K_n}{\bar{c}}\right)^1 = \frac{\pi}{2} \cdot \frac{A}{\frac{dC_{L_W}}{d\alpha}} \cdot \int_{x=-l_t}^{l_n} \frac{b_B^2(x)}{b^2} \cdot \frac{d\beta}{d\alpha} \cdot d\left(\frac{x}{\bar{c}}\right) \quad . . . . . (9)$$

This equation can be evaluated quite simply when the distribution of $\left(\frac{d\beta}{d\alpha}\right)$ along the body is known. Due to thecirculation associated with the bound and trailing vortices downwash exists behind the wing and upwash exists ahead of it, taking downwash as positive

$$\frac{d\beta}{d\alpha} = 1 - \frac{d\varepsilon}{d\alpha} \quad . . . . . (10)$$

The flow is completely guided along the chord and here

$$\frac{d\beta}{d\alpha} = 0$$

The larger contribution to the integral of equation (9) comes from the upwash in front of the wing. Schlichting [11] has modified the equation given by Multhopp [14] for the calculation of the downwash distribution to allow for the effect of sweepback. This modification entails replacing the sweptback wing by a sweptback horse-shoe vortex lying on the wing quarter chord line. As noted in Reference (11) the results obtained for the downwash distribution could be improved by the use of a lifting surface theory. Since lifting line theory has been used in Section 2 of this paper

its use in this calculation should not affect the accuracy of the overall result considerably.

The downwash distribution is given by the expression

$$\frac{d\varepsilon}{d\alpha} = \frac{1}{V} \cdot \frac{dw}{d\alpha} \quad \ldots\ldots\ldots\ldots\ldots\ldots \quad (11)$$

where (V) is the free stream velocity and (w) is the velocity induced by the bound and trailing vortices at the axis of symmetry, and which can be obtained from

$$w = \frac{K}{2\pi s} \cdot \left[1 - \frac{\sqrt{\left(\xi_1 + \tan\varphi\right)^2 + 1} - \frac{\xi_1}{|\xi_1|} \cdot \tan\varphi}{\xi_1} \right] \quad \ldots\ldots \quad (12)$$

where, $K = \frac{1}{2} \cdot \frac{Vb}{A} \cdot \frac{dC_L}{d\alpha} \cdot \delta\alpha$ is the strength of the vortex. The expression for (w) is given in Reference (11) and depends on the plan form of the wing, and $\xi_1 = \frac{x_1}{s}$ where (x_1) is the distance of the point on the body axis from the origin, see Figure (1).

From equations (9), (10), (11), and (12) is obtained the expression

$$\frac{d\beta}{d\alpha} = 1 - \frac{1}{2\pi A} \cdot \frac{dC_L}{d\alpha}_{BW} \left[1 - \frac{\sqrt{\left(\xi_1 + \tan\varphi\right)^2 + 1} - \frac{\xi_1}{|\xi_1|} \cdot \tan\varphi}{\xi_1} \right] \quad \ldots \quad (13)$$

The value of $\frac{dC_L}{d\alpha}_{BW}$ has been used in this expression in preference to that of $\frac{dC_L}{d\alpha}_{W}$ because the body does have an effect on the flow over the exposed wing and

thus has an effect on the downwash distribution along the axis of symmetry. The downwash is being calculated as though the body is not present. This is rather a rough approximation and it is felt that it could be improved slightly by using the lift distribution, and hence the value of $\frac{dC_L}{d\alpha}$, that is obtained for the wing/body combination. The downwash distribution has been calculated for several of the wing/body combinations used in the wind-tunnel tests and the results appear in Figures (17) and (18).

Using the calculated downwash distribution the shift of the aerodynamic centre due to the moment on the body has been calculated and the results have been tabulated in Table (5).

3.4 The total movement of the aerodynamic centre due to the effect of the body can be obtained from

$$\left(-\frac{\Delta K_n}{\bar{\bar{c}}}\right)_{total} = \left(-\frac{\Delta K_n}{\bar{\bar{c}}}\right) + \left(-\frac{\Delta K_n}{\bar{\bar{c}}}\right)^1 \quad \ldots\ldots\ldots \quad (14)$$

The values obtained from this equation appear in Table (6) and are plotted against sweepback in Figure (16). In Figure (15) can be found a comparison of the relevant results from the experimental tests with those obtained by theory. A reproduction of both the theoretical and experimental results published by Schlichting [11] for the variation of the shift of the aerodynamic centre due to the body with the angle of sweepback is given in Figure (14).

In addition, theoretical results have been calculated for the unswept wing/body combinations from both the present series of tests and those used in Reference (8) by the methods of References (4) and (5). These appear in Figures (10) with the corresponding experimental results.

As stated in Reference (3) the lower limit of aspect ratio to which the theory described in the preceding sections may be applied with any accuracy is 2. Thus the agreement between the theoretical and experimental results for the aspect ratio 2 wing may not be very good.

4. DISCUSSION OF THE EXPERIMENTAL RESULTS

It is essential to consider first of all the accuracy which can be expected from the experimental results.

4.1 It was possible, in the experimental work, to measure the Lift, Drag and Pitching Moment accuracies of 0.01 lbs., 0.01 lbs., and 0.02 lb.ins., respectively. The largest errors obtained in the coefficients on repetition of the tests are approximately 0.2/radian in $\frac{dC_L}{d\alpha}$ and 0.01 in $\frac{dC_M}{dC_L}$. The majority of the results are more accurate than this.

In theory, the curve of C_M vs. C_L should be linear up to the stall. The experimental results give curves which undulate about a mean straight line, see Figures (2) to (5). As wide a range of C_L as possible is used to obtain the slope of the mean line, the range being from — 0.8 to + 0.8. The slopes could be calculated mathematically using the method of Least Squares but this method would be too tedious when considering such a volume of data. In any case, obtaining the slope graphically involves the use of an approximate Least Squares method.

From the representative selection of C_M vs. C_L curves given in Figures (2) to (5) the general similarity between them can be seen. At values of C_L near zero the slope of the curve is greater than that of the mean line. At C_L = 0.2 approximately the slope decreases, followed by an increase

in the region of $C_L = 0.4$. It is worthwhile to discuss very briefly the changes in airflow which could cause such a curve.

The effect of Reynolds Number will be discussed later but it can be stated here that the very low Reynolds Number at which the tests were performed makes the prediction of the type of flow existing, laminar or turbulent, and the position of the transition point, extremely difficult. At low C_L the flow could be assumed to be wholly laminar without any separation. At this low Reynolds Number the thickening of the boundary layer which occurs towards the rear of the aerofoil section will cause a loss of lift in this region. This results in the forward movement in the aerodynamic centre [17, 18] which is indicated by the higher than average slope of this portion of the curve. The sudden reduction in the slope in the region of $C_L = 0.2$ shows a loss of lift forward of the mean aerodynamic centre. This loss of lift occurs at the wing root. The local increase in incidence caused by the upwash due to body is most severe at the wing/body junction. This increase in local incidence combined with the discontinuity introduced by the wing root is sufficient to cause very premature local separation of the flow at the wing/body junction with a consequent loss of lift. This region of separated flow, originating at the wing root leading edge, is amply illustrated by the patterns obtained

in the flow visualisation tests, see Figures (19) to (20).

The subsequent increase in the slope of the curve at approximately $C_L = 0.4$ can be associated with a loss of lift behind the mean aerodynamic centre i.e. at the wing tips. Further increase in incidence beyond this value of C_L serves only to increase the area of the separated regions until the wing is completely stalled.

The effect of an increase in the angle of sweepback on the shape of the C_M vs. C_L curve is to decrease the value of C_L at which the changes occur and to increase their severity. Up to an angle of sweepback of 45° it is still possible to draw an accurate mean line in the range of C_L from -0.8 to $+0.8$ but at $\varphi = 60^\circ$ this is impossible, see Figure (5). In this case there is no alternative but to use the short linear portion of the curve between $C_L = -0.2$ and $+0.2$. As has been stated previously the slope of the curve in this region is higher than the average slope and the body appears to cause a greater increase in the value of the slope in this small region than in the mean slope of the curve. Thus, at $\varphi = 60^\circ$ the value of $\left(-\frac{\Delta K_n}{\bar{\bar{c}}}\right)$ due to the body should be overestimated.

The undulations about the mean straight line are till visible for the unswept wings even for the wing alone case. Here the variations can be due only to chordwise

movement of the aerodynamic centre broughtabout by the transition of the flow from laminar to turbulent and the developement of regions of separated flow. These factors will be present for the sweptback wings as well but in these cases the relative geometrical positions of the separated regions will have the predominant effect.

Every effort has been made to ensure consistency in the limits of the range of C_L over which the slope of C_M vs. C_L is measured. Although the absolute values of the slope of the C_M vs. C_L curves, as obtained by drawing a mean straight line, could be challenged, the difference between two such values, which is the only value of interest in this paper, should be reasonably accurate.

4.2 It becomes apparent when comparing the experimental curves obtained in this series of tests with those of other papers that the low Reynolds Number employed here has a major effect on the absolute value of $\frac{dC_M}{dC_L}$. Its effect on the value of $\left(\Delta \frac{dC_M}{dC_L}\right)$ due to a body is very much more difficult to define since there is no means of comparing the effect of the addition of the body at different Reynolds Numbers.

Reference (19) compares curves of C_M vs. C_L at different Reynolds Numbers. The configuration is a wing/body combination but unfortunately the corresponding curves for the wing alone are not given. The curve of C_M vs. C_L at R.N. = 0.52×10^6 is very similar in general shape to those

obtained in the present tests, while that given for R.N. = 4.85×10^6 is markedly different, being of reduced slope and considerably more linear up to the stall. The effect of increasing the Reynolds Number beyond that used in this series of tests would appear to be that of moving the aerodynamic centre rearwards and alleviating the sudden losses of lift at wing root and tip.

Estimation of the effect of Reynolds Number on $\left(\Delta \frac{dC_M}{dC_L}\right)$ due to a body without any experimental evidence is extremely difficult. An increase in Reynolds Number affects the flow over the wing alone as well as that over the wing/body combination so the problem reduces to the consideration of the flow over that part of the wing influenced by the body and over the body itself. This excludes the wing tips except at very low aspect ratios since the body effect becomes negligible at more than a chord's length from the wing/body junction.

The effect of an increase in Reynolds Number on the flow over the body should be to reduce the area of the region of separated flow over the rear of the body. This should cause an increase in the download and hence an increase in the destabilising nose-up moment. The flow at both the axis of symmetry of the wing alone and at the wing root of the wing/body combination should be improved by an increase in Reynolds Number. The magnitudes of all these effects are very difficult to estimate. In fact it does not appear to

be too unreasonable to assume that at this low Reynolds Number the loss of lift at the centre section of the wing alone is greater than the lift loss at the wing roots of the wing/body junction. The introduction of the body on to the wing alone would remove the region of separated flow and the improvement need not be cancelled out by the disturbance at the wing roots. The poor flow at the centre section of the wing alone would be reflected in a negative value for $\frac{dC_M}{dC_L}$ and a resultant overestimation of the effect of the body on the position of the aerodynamic centre.

4.3 Before going on to discuss experimental results in detail the effect of the support system used in the tests will be briefly considered.

The tests performed with an image of the support system in place do not show any material change in the values of $\left(\Delta\frac{dC_M}{dC_L}\right)$. This does not necessarily mean that the support system has no effect on the flow. Rather, it may be that the flow over the centre section of the wing alone and over the body of the wing/body combination is already so disturbed that the introduction of the image support system does not cause any appreciable change.

It is felt that, in principle, the use of a single main support is not suitable when determining the influence of the body on any of the aerodynamic coefficients. Ideally the model should always be mounted such that the main supports are outside the region influenced by the body. The effect of

of the support on the wing alone and on the body will not then enter into the results at all, since it is the difference between these two cases which is considered.

4.4 The effects of sweepback and aspect ratio on the shift of the aerodynamic centre due to a body appear in Figure (6). The equivalent results from References (8), (9) and (10) are plotted in Figure (11) and those from Reference (11) in Figure (14). The results obtained in the present tests will be compared with those of Figures (11) and (14) in the following sections.

4.41 The results of Figure (11) will be discussed first of all. At a first glance the agreement between the two sets of results is not very good except for the unswept wings. The discrepancy increases with increase in the angle of sweepback. It is therefore most important to point out that the differences between the model configurations and Reynolds Numbers of the two series of tests are such that the results are not directly comparable.

In the first place a certain amount of doubt exists concerning the accuracy of the results shown in Figure (11). The values in References (8), (9) and (10) are given in the form of small scale graphs with widely spaced points. Replotting these points on a larger scale leaves a margin for error and gives curves whose slopes are difficult to determine accurately. The results in Figure (11) are given as discrete points without connecting lines since the values

of $\left(\frac{\Delta K_n}{\bar{c}}\right)$ for $\varphi = 30^\circ$ are not available, and lines drawn without these points would not be very reliable.

The results of References (8), (9) and (10) are based on a constant wing area, thus the root chord decreases with increase in aspect ratio and hence the ratio of the body nose length against root chord increases in aspect ratio. This produces the effect that movement of the aerodynamic centre due to the body with increase with aspect ratio will be proportionately larger than in the case where the root chord remains of constant length.

In addition, the mean aerodynamic centre is maintained at an approximately constant distance behind the body nose as the angle of sweepback increases. Thus the distance of the root quarter chord point from the body nose decreases with increase in sweepback. This results in the body having a smaller effect as sweepback increases than the case in which the root quarter chord point is maintained in a constant position. This is the most important variable and the reason for this will be discussed in a later section.

The wing/body combinations of the present paper use a constant wing chord with variation in aspect ratio and sweepback and maintain a constant quarter chord position. If the two sets of results are to be compared then it is to be expected that the results of Figure (11) will show much less variation with increase in aspect ratio and a larger variation in the body effect with increase in sweepback than

the results shown in Figure (6). As can be seen, this is in fact correct.

The differences in the effect of aspect ratio are borne out by the curves given in Figure (10) where it can be seen that for the unswept wings the values obtained for both the present series and for Reference (8) are predicted quite well by the theory of References (4) and (5). Figure (7) shows that, from the present experimental results, forward movement of the wing root chord position on a body of constant length results in a reduction in body effect which increases slightly with increase in sweepback.

These two effects together with the difference in Reynolds Number between the two series would appear to account for the discrepancies which exist between the two sets of results. Although the results shown in Figure (11) must be treated with a certain amount of caution they may be considered as showing more or less the same trends as those of Figure (6).

4.42 When comparing the experimental results of Figure (6) with those of Reference (11) given in Figure (14) it is necessary to comment, as before, that the two sets of results are not directly comparable due to differences in model configuration and Reynolds Number.

In this case the wing root chord is maintained of constant length but the root chord position is treated in two different ways. One is that the axis of symmetry quarter

chord point is maintained in a constant position so that the root chord moves back slightly with increase in sweepback and the other is similar to the case of Figure (11) where the mean aerodynamic centre is kept in a constant position. The first case in the one which corresponds more closely to the configurations of the experimental work of this paper. Following a similar reasoning to that of the previous section, since the root chord moves back with an increase in sweepback in Figure (14) then the results of this Figure should be slightly greater than those of Figure (6) as sweepback increases. However this is not shown by the comparison of the figures since the body nose length employed in the present series is considerably larger than that used in Reference (11). The result is that the results of this present series, as shown in Figure (6) and (15) give larger values for $\left(-\frac{\Delta K_n}{\bar{c}}\right)$ than those of Reference (11), as given in Figure (14), except for the unswept wings. The discrepancy increases with increase in sweepback.

As before the effect of uncertain magnitude of the difference in Reynolds Number is present. Again, as in Section 4.41, it is necessary to treat the results of Reference (11) with caution as they are not directly comparable but it would appear that it is possible to find a reasonable explanation for the discrepancies that do exist.

So far no mention has been made of the forms of the curves in Figure (6) in the region of $\varphi = 60^{\circ}$. Although these

do not compare with either Figures (11) or (14) they need not diminish in any way the accuracy of the general trends shown by the curves. The curves of Figure (6) will be discussed in more detail in a later section.

4.43 To sum up the discussion of Sections 4.41 and 4.42 it may be said that although the results are not directly comparable no trends are shown which are at variance with those of the present experimental tests.

The slopes of the curves of $\left(-\frac{\Delta K_n}{\bar{\bar{c}}}\right)$ vs. $\cos\varphi$ increase through the Figures (14), (11) and (6). This is caused by the differences in the model configurations, the most important being that of the body nose length measured from the root quarter chord point. Figure (14) is based on a model of an approximately constant nose length but which is considerably shorter than the other two series of models. Figure (11) is based on a model with a nose length that is nearly equal to that of the model of Figure (6) but which decreases rapidly with increase in sweepback. Figure (6) is based on a model of constant nose length.

The increase in the ratio of body nose length against root chord with aspect ratio in Figure (11) produces a much smaller change in $\left(-\frac{\Delta K_n}{\bar{\bar{c}}}\right)$ with increase in aspect ratio than that of Figure (6) which employs a constant ratio. The influence of Reynolds Number or the use of tapered wings cannot be clearly defined but the Reynolds Number may be important.

In general, an increase in the angle of sweepback, and to a lesser extent an increase in aspect ratio cause a decrease in the value of $\left(-\frac{\Delta K_n}{\bar{\bar{c}}}\right)$ due to a body.

4.5 In figure (15) will be found a comparison of the experimental results with those of the theoretical analysis used in this paper. It can be seen that the agreement is reasonably good over the ranges of sweepback and aspect ratio covered. The general trend is however that the experimental results are higher than the theoretical ones except for the unswept wings.

For the unswept wings the theory of the present paper agrees well with both the experimental results and the theory of References (4) and (5). The experimental value for the wing of aspect ratio 2 is a little high but then this aspect ratio is the limit for the application of this type of method. At the angles of sweepback of 30° and 45° the experimental results are rather high but study of Table (2) shows the reason for the discrepancies. The values of $\frac{dC_M}{dC_L}$ in each case for the wing alone are negative instead of being zero. This indicates that there is severe loss of lift at the centre section of the wing alone. Addition of the body covers this region of low lift and the apparent change in $\frac{dC_M}{dC_L}$ overestimates the true value. The possibility of this occurrence was mentioned in Section 4.2.

At $\varphi = 60^\circ$ there is a complete reversal in the effect of aspect ratio. This is not predicted in theory or

shown by any other results. A possible answer is that, as mentioned in Section 4.1, at this angle of sweepback it is neccesary to use the short linear portion of the curve close to $C_L = 0$ in order to obtain a value for the slope. It is possible that at such a high angle of sweepback the flow over the wing alone at the lower aspect ratios is already so far removed from the theoretical two-dimensional state that the addition of the body does not produce such a large change in $\frac{dC_M}{dC_L}$ as it does on wings of a larger aspect ratio where the flow is slightly more stable. The very high angle of sweepback brings more of the wing into the upwash around the body and the area of disturbed flow will be larger than on less sweptback wings. The moment arm about the mean aerodynamic centre of the regions of separated flow will also be greater.

In Figure (14) both the experimental and theoretical results from Reference (11) can be seen. At low angles of sweepback the theory predicts the experimental results fairly well but by $\varphi = 45^\circ$ the error is appreciable and appears to be increasing with further increase in sweepback. The results of the present method, as shown in Figure (15), do predict quite accurately the experimental results at the higher aspect ratio. The error for the unswept wing is very small and those at $\varphi = 30^\circ$ and 45° have already been explained. The increase in $\left(-\frac{\Delta K_n}{\bar{\bar{c}}}\right)$ at $\varphi = 60^\circ$ is also predicted without serious loss in accuracy.

This rise in $\left(-\frac{\Delta K_n}{\bar{\bar{c}}}\right)$ for the larger value of aspect ratio in the higher ranges of sweepback is not shown by the experimental results of References (9), (10) or (11). It is obviously dependent on the actual configuration and as can be seen the theoretical analysis predicts the rise quite well. It would appear then that the modifications made to the theory of Reference (11) have been beneficial to its accuracy.

Table (4) compares the moments due to the loss of wing lift due to the body as calculated by the methods of Reference (11) and the present method. The differences are due to the modifications made to the theory in the present method. The main alteration is that the spanwise lift distribution and the lift curve slope are calculated for each case rather than purely for the unswept wing as in Reference (11). It can be observed that at the higher aspect ratio a slight decrease in the magnitude of the moment due to loss of wing lift is predicted at $\varphi = 60^{\circ}$.

Table (5) shows the values obtained for the moment due to the lift on the body. It also shows the effect of assuming separation of the flow at the wing root trailing edge as distinct from no flow separation at all. As expected, any separation of the flow over the rear of the body causes a reduction in the download and hence a reduction in $\left(-\frac{\Delta K_n}{\bar{\bar{c}}}\right)$. This is illustrated in Figure (12).

From a comparison of Figures (14) and (15) it may be observed that the same basic theory agrees quite well with the experimental curves obtained from two different wing/body combinations. This indicates that the actual configuration plays an important part in the magnitude of the wing/body interference effect, especially at high angles of sweepback.

4.6 The change in body effect produced by altering the body nose length while maintaining a constant tail length appears in Figure (8). The results agree with those of Reference (4) in that the variation of $\left(-\frac{\Delta K_n}{\bar{\bar{c}}}\right)$ is linear and of positive slope with increase in nose length. The agreement between the aspect ratio 4 wing of this paper and the wing of aspect ratio 5 in Reference (4) is quite good. Bearing in mind the slight overestimation of the values for $\varphi = 45^\circ$ the effect of sweepback is to reduce the slope of the curves.

From Table (3) can be extracted the variation of $\left(-\frac{\Delta K_n}{\bar{\bar{c}}}\right)$ with increase in tail length. Only two points for each case are available but it can be seen that an increase in tail length causes a slight increase in $\left(-\frac{\Delta K_n}{\bar{\bar{c}}}\right)$. This indicates that there is a certain amount of download generated by the rear of the body, suggesting that separation does not occur until aft of the junction between the cylindrical body and conical tail piece.

The body nose length is the dominant factor, the tail length having only a secondary effect. This is because of the distribution of upwash and downwash produced by the circulation round the wing. As has been explained in a previous section the upwash ahead of the wing increases the effective incidence of the body nose while the downwash behind it decreases the effective incidence of the tail. The lift distribution along the body which causes the resultant pitching moment, is dependent on the local incidence and hence the influence of body nose is greater than that of the tail. This results in a movement of the wing root position forward causing a decrease in the value of $\left(-\frac{\Delta K_n}{\bar{\bar{c}}}\right)$. The decrease increases with sweepback as illustrated in Figure (7).

4.7 An increase in body diameter or in the ratio of body diameter to wing span causes an increase in body effect, as shown in Figure (9). Again bearing in mind the overestimation at $\varphi = 45^{\circ}$ the effect of sweepback is to reduce the magnitude of the results while maintaining the shape of the curves. Inspection reveals that the variation of $\left(-\frac{\Delta K_n}{\bar{\bar{c}}}\right)$ with diameter is slightly greater than D^2. Reference (4) gives the variation as just under D^2 while theoretically the value should be D^2. The discrepancy could be a factor of Reynolds Number and generally poor flow conditions.

4.8 The flow visualization tests that were performed were not very successful. They were confined to the angles of sweepback of 45° and 60° to try to find some visual evidence of the reversal of the effect of aspect ratio which was found to occur. Some sketches of the flow patterns obtained using tufts are shown in Figure (19).

As can be seen little useful information can be obtained from these tests. They serve mainly to illustrate the regions of separated flow at the wing root and tip and the disturbance caused at the rear of the body by the main support and shield. There is no radical alteration in the flow pattern on increasing the aspect ratio at either angle of sweepback. At this low Reynolds Number the tufts themselves may have some effect on the flow. The point of separation of the flow at the rear of the body is not clearly defined at all but is somewhere in the region of the junction of the conical tail section and the cylindrical centre section.

The patterns observed in the tuft tests correspond quite closely to those given in Reference (21). A suggestion for improving the flow conditions at the wing root is given in Reference (20). The improvement is effected by altering the body width along the chord to follow the assumed path of the streamlines. This alleviates the high suction peak and consequent strong adverse pressure gradient that exists in the wing/body junction.

4.9 In table (4) there appear the values of $\frac{dC_L}{d\alpha}$ which were obtained in the course of the calculation of $\left(-\frac{\Delta K_n}{\bar{\bar{c}}}\right)$ due to the loss of wing lift. The values were obtained by the same method as in Reference (3) and so of course correspond almost exactly.

Reference (3) also discusses the vorticity vector which represents the circulation around the wing. For the purposes of the theoretical method the vector is depicted by a horse—shoe vortex made up of straight lines. With a sweptback wing the horse—shoe is bent at the axis of symmetry see Figure (1). In actual fact however the vorticity vector should cross the axis at right angles. This is inherent in the unswept wing but for the sweptback wing the vector must curve, see Figure (1). This involves a backward movement of the point at which the vector cuts the axis and results in vortices being shed near the axis of symmetry which are of opposite sense to those along the rest of the semispan.

These trailing vortices of opposite sense reduce the downwash along the axis of symmetry and hence increase the effective angle of incidence of the tail of the body. This in turn will increase the value of $\left(-\frac{\Delta K_n}{\bar{\bar{c}}}\right)$ due to the body and will become more pronounced with increase in the angle of sweepback.

This effect is not predicted by the theoretical work and will contribute considerably to the discrepancy of underestimation by the theoretical results for the sweptback wings, especially at the higher angles of sweepback.

5. CONCLUSIONS

It would appear from the foregoing discussion that the experimental work performed for this paper has produced some useful results. It must always be borne in mind that both the Reynolds Number and the system used to support the models are a little unsuitable for the production of reliable, quantitative results.

The comparison of the experimental results with those of the papers considered shows no trends which are in disagreement with each other. The differences that do exist are factors of the configurations of the various wing/body combinations. The modifications that have been made to the previous theory appear to have been beneficial since the agreement with the experimental results is closer, especially at the higher angles of sweepback.

For the results obtained in this paper it would appear to be unwise to make quantitative generalisations concerning the effect of sweepback on the wing/body interference effect. Each type of wing/body combination must be treated on its own merits. In spite of this it can be stated that in general, for low angles of sweepback, an increase in the angle of sweepback will produce a decrease in the forward movement of the aerodynamic centre due to a body. In the higher ranges of sweepback each wing/body combination must be treated individually because of the increased influence of the type of configuration. The effect

of aspect ratio is of less importance. In general an increase in aspect ratio reduces the influence of the body. This is of course coupled with the variation of the ratio of body diameter to span.

Of the body parameters the body nose length and the ratio of body diameter to wing span are the most important. An increase in either produces an increase in the influence of the body.

The effect of Reynolds Number on the influence of the body is difficult to define due to the lack of experimental evidence. It would be extremely useful to repeat the tests done here at a much higher Reynolds Number to clarify the situation. At the same time it would be advisable to modify the support system to remove the main support strut from the region of the influence of the body to further improve the accuracy of the results.

The experimental work done in this paper could be extended to cover tapered wings and delta wing/body combinations to investigate the influence of wing/body interference on both the lift curve slope and the position of the aerodynamic centre. The accuracy of the theoretical analysis could be improved by incorporating a lifting surface theory into the calculation of the lift distribution on the wing in the presence of a body and the downwash distribution along the axis of symmetry. The theoretical

work could be extended to cover tapered wings and delta wing/body combinations to keep pace with the experimental work. Further work could be done to extend the theory to cover aspect ratios of less than two which is the present lower limit.

REFERENCES

1.	H. Schlichting	Aerodynamics of the mutual influence of aircraft parts (interference). R.A.E. Lib. Trans. 275. 1948.
2.	H.R. Lawrence and A.H. Flax	Wing/body interference at subsonic and supersonic speeds — survey and new developments. Journal of the Aeronautical Sciences Vol. 21. No. 5. p.p. 289–323. 1954.
3.	B. Blair	M.Sc. Thesis. Glasgow University 1961.
4.	A. Anscombe and D.J. Raney	Low Speed Tunnel investigation of the effect of the body on C_{M_O} and Aerodynamics Centre of Unswept Wing/Body combinations C.P. 16. 1950.
5.	R. Ae. Soc.	Data Sheets — Aerodynamics Vol. 3.
6.	A. Pope	Wind Tunnel Testing.
7.	W.E.A. Acum	Corrections for Symmetrical Sweptback and Tapered wings in rectangular wind tunnels.
8.	W.D. Wolhart and D.F. Thomas	Static Longitudinal and Lateral stability characteristics at low speed of unswept–midwing models having wings with an aspect ratio of 2, 4 or 6. NACA TN 3649 1956.
9.	D.F. Thomas and W.D. Wolhart	Static Longitudinal and Lateral stability characteristics at low speed of 45° sweptback midwing models having wings with an aspect ratio of 2, 4 or 6. NACA TN 4077 1957.
10.	W.D. Wolhart and D.F. Thomas	Static Longitudinal and Lateral stability characteristics at low speed of 60° sweptback midwing models having wings with an aspect ratio of 2, 4 or 6. NACA TN 4397 1958.

11. H. Schlichting — Calculation of the influence of a body on the position of the aerodynamic centre of aircraft with sweptback wings.

12. H. Multhopp — Aerodynamics of the fuselage. R.T.P. Trans. No. 1200 1941.

13. J. Weber, D.A. Kirby, and D.J. Kettle — An extension of Multhopp's method of calculating the spanwise loading of wing/fuselage combination. R.&M. 2872 1951.

14. H. Multhopp — The calculation of the lift distribution of aerofoils. R.T.P. Trans. No. 2392. 1938.

15. D. Kuchemann — A simple method for calculating the span and chordwise loadings on thin swept wings. Report Aero 2392 1950.

16. M.M. Munk — The aerodynamic forces on airship hulls. NACA Report No. 184. 1924.

17. J. Weber — Balance measurements on two 45° sweptback wing of aspect ratio 3 at Reynolds Numbers varying between 0.5×10^6 and 12×10^6 T.N. Aero 2257

18. D. Kuchemann, J. Weber, and G.G. Brebner — Low speed tests on 45° sweptback wings. R.&M. 2882 1958.

19. Salter, Miles, and Lee — Tests on a sweptback wing and body in the compressed air tunnel. R.&M. 2738 1953.

20. D. Kuchemann, and J. Weber — The subsonic flow past a swept wing at zero lift without and with a body. R.&M. 2908 1956.

21. P.E. Purser, and M. Leroy Spearman — Wind tunnel tests at low speed of swept and yawed wings having various plan-forms NACA TN 2445 1951.

Appendix (I)

There follows a simplified flow diagram for the programme used to analyse the wind tunnel data.

$$C_L = \frac{L}{q.S}$$

$$C_D = \frac{D}{q.S}$$

$$C_{M_{\frac{c}{4}}} = \frac{1}{q.S.\bar{\bar{c}}} . M_r + L.h.\bar{\bar{c}}$$

where, h = distance from measuring point to mean aerodynamic centre.

M_r = Pitching moment about measuring point.

$C_{M_{\frac{c}{4}}}$ = Pitching moment about mean quarter chord point.

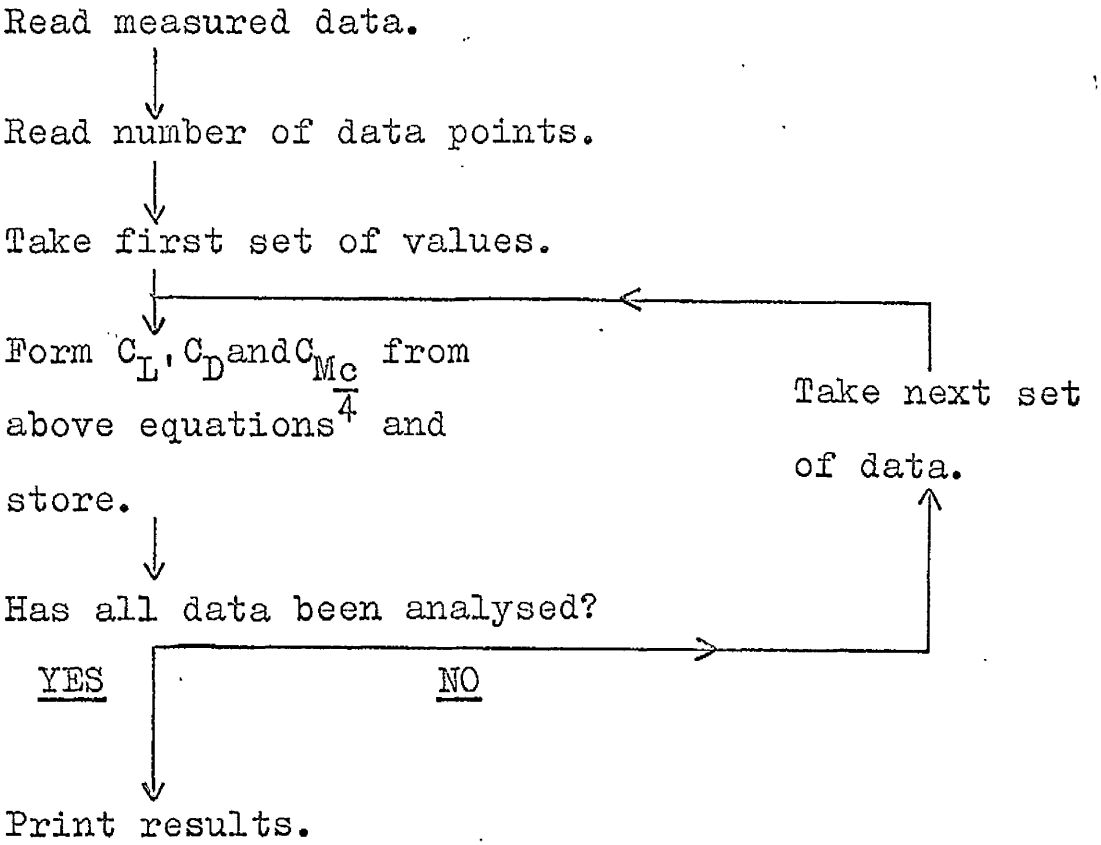

APPENDIX (II)

Below is a much simplified flow diagram of the programme used calculate the forward movement of the aerodynamic centre due to the influence of a body, $\left(-\frac{\Delta K_n}{\bar{\bar{c}}}\right)$. Only the sources for the equations and their derivations are given in the flow diagram. Unless otherwise stated it may be assumed that the equation numbers apply to this paper.

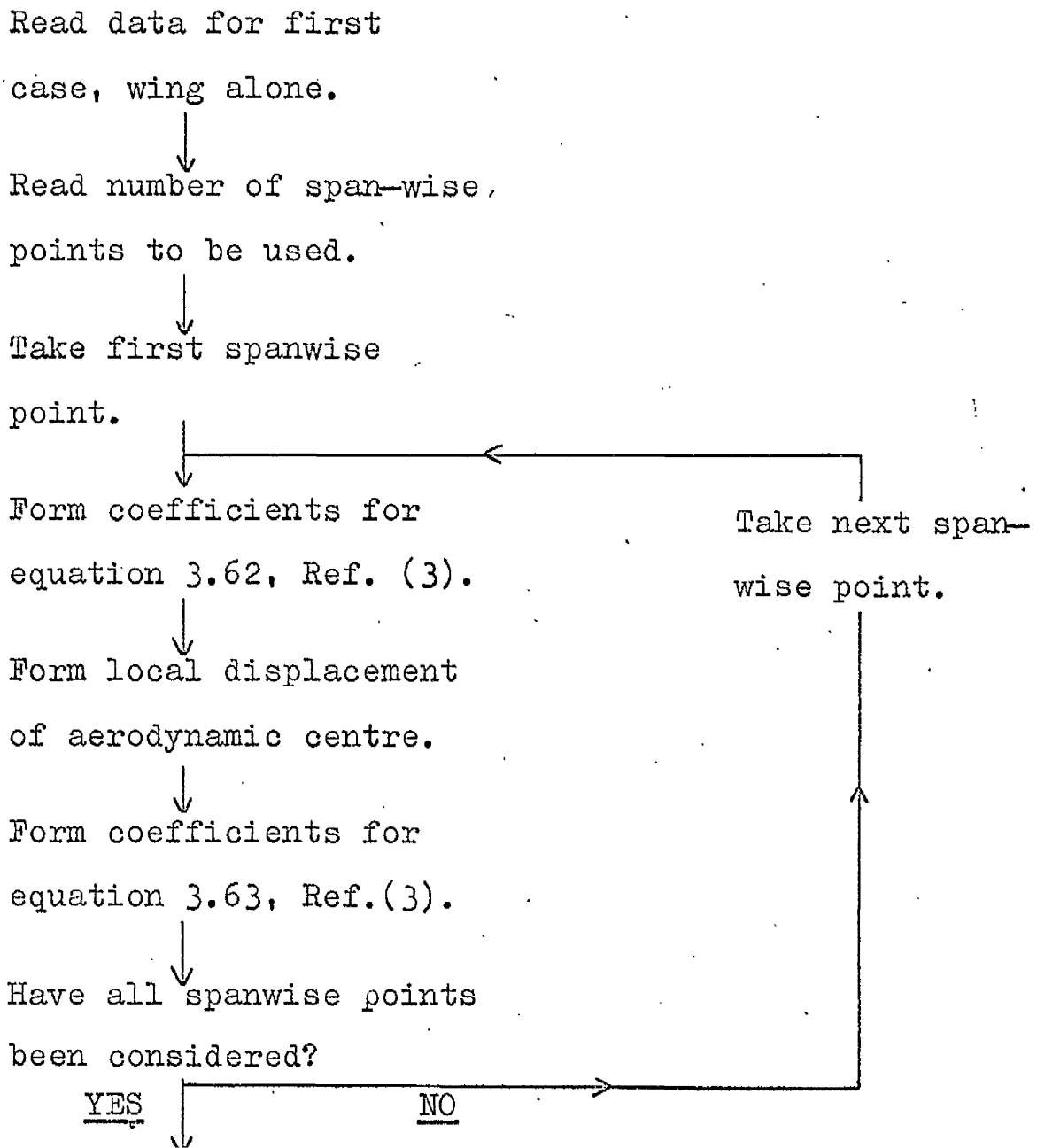

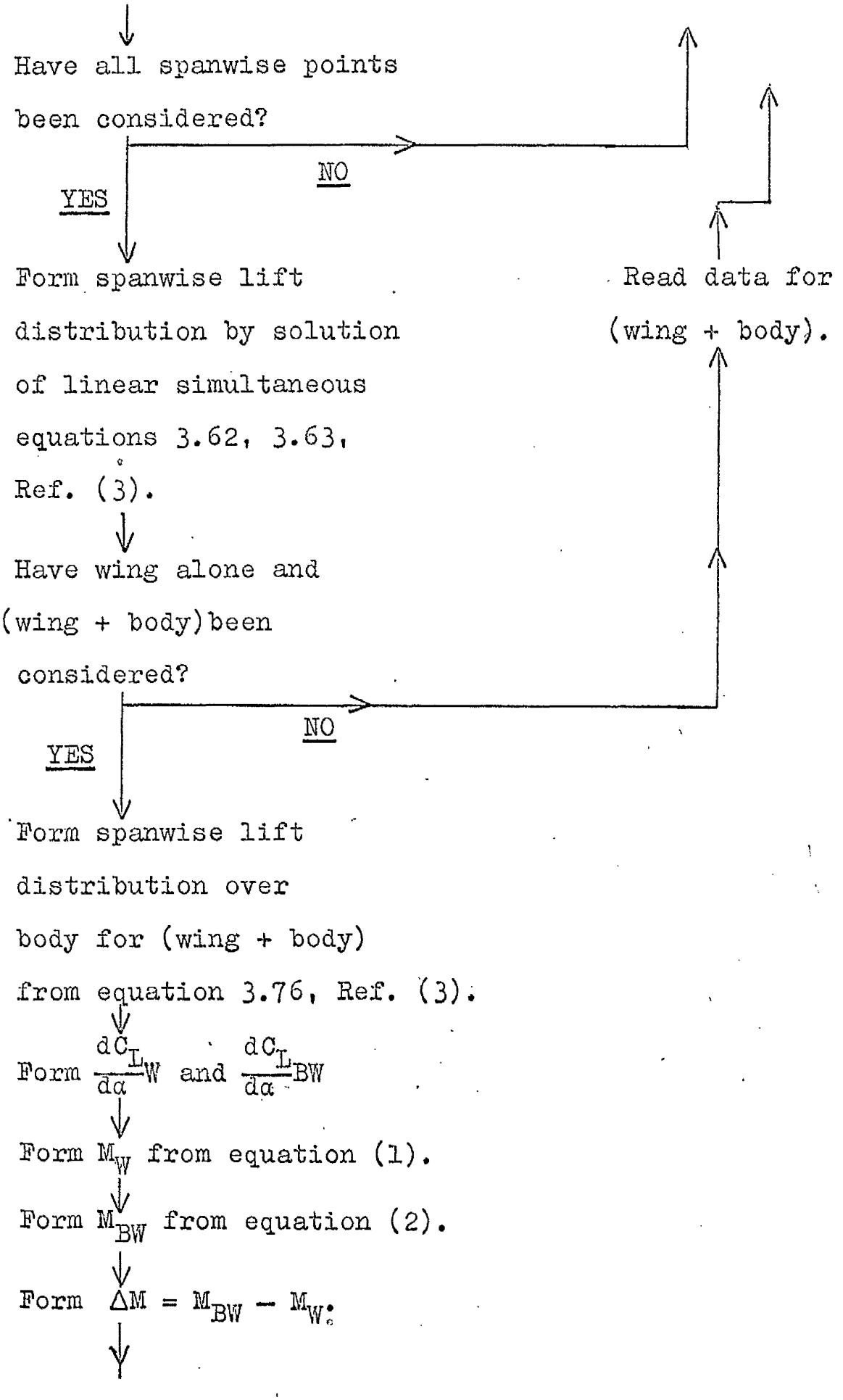
Have all spanwise points been considered?
NO
YES
Read data for (wing + body).
Form spanwise lift distribution by solution of linear simultaneous equations 3.62, 3.63, Ref. (3).
Have wing alone and (wing + body) been considered?
NO
YES
Form spanwise lift distribution over body for (wing + body) from equation 3.76, Ref. (3).
Form $\frac{dC_L}{d\alpha}_W$ and $\frac{dC_L}{d\alpha}_{BW}$
Form M_W from equation (1).
Form M_{BW} from equation (2).
Form $\Delta M = M_{BW} - M_W$.

Form $\left(-\frac{\Delta K_n}{\bar{c}}\right)$ due to loss of wing lift from equation (4) and store.

Read number of points on axis of symmetry for downwash distribution.

Take first point.

Form $\frac{d\beta}{d\alpha}$ from equation (13).

Form value of integral part of equation (9) and plot.

Have all points on axis of symmetry been considered?

NO → Take next point

YES

Find area under integral curve of equation (9).

Form $\left(-\frac{\Delta K_n}{\bar{c}}\right)^l$ due to lift on body from equation (9).

Form $\left(-\frac{\Delta K_n}{\bar{c}}\right)_{total} = \left(-\frac{\Delta K_n}{\bar{c}}\right) + \left(-\frac{\Delta K_n}{\bar{c}}\right)^l$.

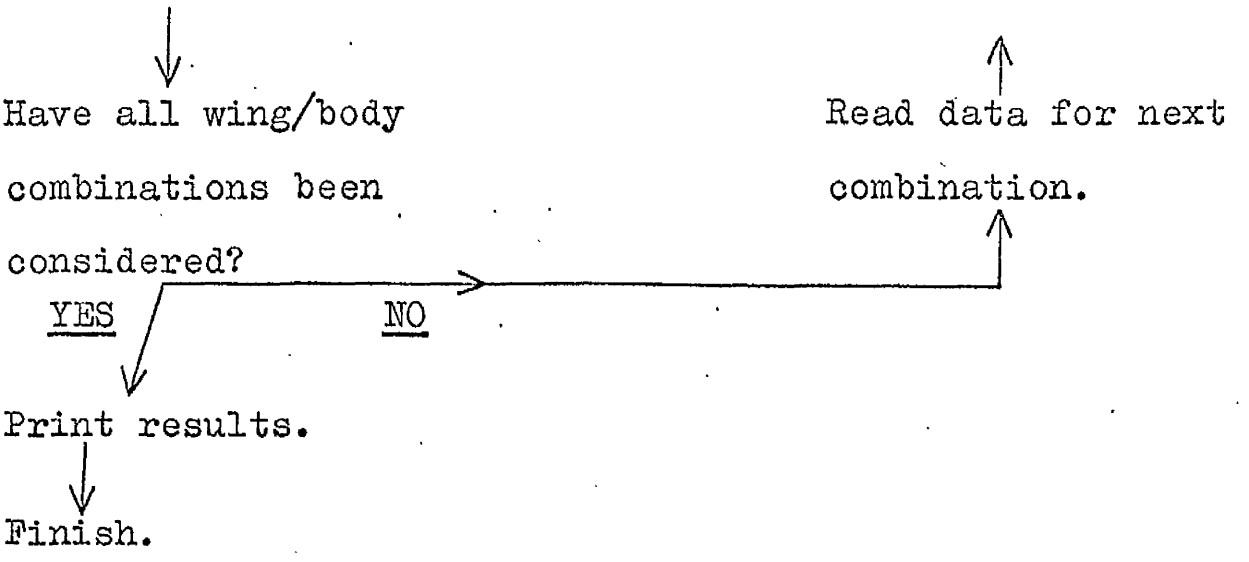
Have all wing/body combinations been considered?
YES
NO
Read data for next combination.
Print results.
Finish.

BODY	F^1_{22}	F^1_{12}	F^1_{11}	F^1_{21}	F^1_{31}	F^2
NOSE LENGTH (INS)	11	8	8	11	14	17.4
TAIL LENGTH (INS)	16.5	16.5	13.6	13.6	13.6	23.9
TOTAL LENGTH (INS)	27.5	24.5	21.6	24.6	27.6	41.3
$\frac{M}{C}$	1.583	1.083	1.083	1.583	2.084	2.650
$\frac{N}{C}$	2.000	2.000	1.520	1.520	1.520	3.235
$\frac{L_N}{L_B}$	0.400	0.327	0.370	0.447	0.508	0.422

Body configurations are represented by the symbol F^a_{bc}, superscript (a) indicating the diameter and the subscript showing the number of sections in the nose (b) and the tail (c).

Wing configurations are represented by the symbol W^x_y, superscript (x) indicating the angle of sweepback in degrees and the subscript showing the aspect ratio.

ASPECT RATIO	2	3	4	5
SPAN (FT)	1	1.5	2	2.5
AREA (SQ.FT)	0.50	0.75	1.00	1.25
CHORD (FT)	0.5	0.5	0.5	0.5

TABLE (1). Wing and body configurations.

BODY / WING	0	F^1_{22}	F^1_{12}	F^1_{11}	F^1_{21}	F^1_{31}	F^2
W^0_2	0.000	0.160	0.126	0.107	0.142	0.181	0.506
W^0_3	0.000	0.104	0.107	0.074	0.103	0.115	0.252
W^0_4	0.000	0.054	0.044	0.037	0.044	0.053	0.177
W^{30}_2	$\bar{0}$.030	0.135	0.093	0.065	0.102	0.142	0.596
W^{30}_3	$\bar{0}$.036	0.085	0.058	0.051	0.069	0.091	0.233
W^{30}_4	$\bar{0}$.038	0.063	0.047	0.042	0.056	0.066	0.180
W^{30}_5	$\bar{0}$.045	0.054	0.040	0.038	0.050	0.052	0.142
W^{45}_2	$\bar{0}$.033	0.078	0.042	0.052	0.080	0.106	0.310
W^{45}_3	$\bar{0}$.022	0.057	0.040	0.034	0.053	0.082	0.218
W^{45}_4	$\bar{0}$.027	0.047	0.035	0.038	0.047	0.061	0.165
W^{45}_5	$\bar{0}$.019	0.037	0.041	0.036	0.039	0.055	0.143
W^{60}_2	0.000	0.050	0.014	0.000	0.052	0.080	0.321
W^{60}_3	0.000	0.082	0.050	0.052	0.097	0.127	0.263
W^{60}_4	0.000	0.100	0.086	0.064	0.133	0.138	0.210
W^{60}_5	0.000	0.119	0.104	0.093	0.159	0.181	0.189

TABLE (2). $\frac{dC_M}{dC_L}$ for wing/body combinations

BODY / WING	0	F^1_{22}	F^1_{12}	F^1_{11}	F^1_{21}	F^1_{31}	F^2
W^0_2	0.000	0.160	0.126	0.107	0.142	0.181	0.506
W^0_3	0.000	0.104	0.107	0.074	0.103	0.115	0.252
W^0_4	0.000	0.054	0.044	0.037	0.044	0.053	0.177
W^{30}_2	0.000	0.165	0.123	0.099	0.132	0.172	0.626
W^{30}_3	0.000	0.121	0.094	0.087	0.105	0.127	0.269
W^{30}_4	0.000	0.101	0.085	0.080	0.094	0.104	0.218
W^{30}_5	0.000	0.099	0.085	0.083	0.095	0.097	0.187
W^{45}_2	0.000	0.111	0.075	0.085	0.113	0.139	0.343
W^{45}_3	0.000	0.079	0.062	0.056	0.075	0.104	0.240
W^{45}_4	0.000	0.074	0.062	0.065	0.074	0.088	0192
W^{45}_5	0.000	0.056	0.060	0.055	0.058	C.074	0.162
W^{60}_2	0.000	0.050	0.014	0.000	0.052	0.080	0.321
W^{60}_3	0.000	0.082	0.050	0.052	0.097	0.127	0.263
W^{60}_4	0.000	0.100	0.086	0.064	0.133	0.138	0.210
W^{60}_5	0.000	0.119	0.104	0.093	0.159	0.181	0.189

TABLE (3). $\left(\Delta \frac{dC_M}{dC_L}\right)$ for wing/body combinations

WING	$\left(-\frac{\Delta K_n}{\bar{\bar{c}}}\right)$ (a)	$\left(-\frac{\Delta K_n}{\bar{\bar{c}}}\right)$ (b)	φ
W_2^0	0.0000	———	
W_4^0	0.0000	0.0000	0°
W_2^{30}	$\bar{0}$.0252	———	
W_4^{30}	$\bar{0}$.0199	$\bar{0}$.0607	30°
W_2^{45}	$\bar{0}$.0385	———	
W_4^{45}	$\bar{0}$.0256	$\bar{0}$.1050	45°
W_2^{60}	$\bar{0}$.0505	———	
W_4^{60}	$\bar{0}$.0220	$\bar{0}$.1820	60°

(a) Present method. Untapered wing, body $-\frac{D}{b} = 0.125$.

(b) Reference (11). Untapered wing, aspect ratio = 5, body $-\frac{D}{b} = 0.143$.

TABLE (4). Moment due to loss of wing lift. (cont. over)

WING	$\left(\frac{dC_L}{d\alpha}\right)_W$ (a)	$\left(\frac{dC_L}{d\alpha}\right)_{BW}$ (a)	$\left(\frac{dC_L}{d\alpha}\right)_W$ (b)	$\left(\frac{dC_L}{d\alpha}\right)_{BW}$ (b)	φ
W_2^0	3.02	2.86	——	——	
W_4^0	4.00	4.14	4.28	3.65	0°
W_2^{30}	2.76	2.67	——	——	
W_4^{30}	3.57	3.72	4.28	3.65	30°
W_2^{45}	2.48	2.46	——	——	
W_4^{45}	3.10	3.25	4.28	3.65	45°
W_2^{60}	2.07	2.14	——	——	
W_4^{60}	2.45	2.58	4.28	3.65	60°

(a) As in previous page.

(b) As in previous page.

TABLE (4). Moment due to loss of wing lift. (concl.)

WING	$\left(-\frac{\Delta K_n}{\bar{\bar{c}}}\right)(a_1)$	$\left(-\frac{\Delta K_n}{\bar{\bar{c}}}\right)(a_2)$	$\left(-\frac{\Delta K_n}{\bar{\bar{c}}}\right)(b)$	φ
W_2^0	0.1455	0.1248	——	
W_4^0	0.0628	0.0528	0.071	0°
W_2^{30}	0.1490	0.1228	——	
W_4^{30}	0.0638	0.0475	0.0623	30°
W_2^{45}	0.1605	0.1265	——	
W_4^{45}	0.0701	0.0526	0.0523	45°
W_2^{60}	0.1820	0.1305	——	
W_4^{60}	0.0821	0.0573	——	

(a_1) Conditions as in (a) Table (4). Body – $\frac{L_N}{L_B} = 0.508$
No breakaway.

(a_2) Conditions as in (a) Table (4). Body – $\frac{L_N}{L_B} = 0.508$
Breakaway at the wing root trailing edge.

(b) Conditions as in (b) Table (4). Body – $\frac{e}{l_b} = 0.3$
No breakaway.

TABLE (5). Forward movement due to lift on body.

WING	$\left(-\frac{\Delta K_n}{\bar{\bar{c}}}\right)(a_1)$	$\left(-\frac{\Delta K_n}{\bar{\bar{c}}}\right)(a_2)$	$\left(-\frac{\Delta K_n}{\bar{\bar{c}}}\right)(b)$	φ
W_2^0	0.1455	0.1248	———	
W_4^0	0.0628	0.0528	0.0710	0°
W_2^{30}	0.1338	0.0976	———	
W_4^{30}	0.0439	0.0276	0.0020	30°
W_2^{45}	0.1220	0.0880	———	
W_4^{45}	0.0445	0.0270	0.0527	45°
W_2^{60}	0.1315	0.0800	———	
W_4^{60}	0.0600	0.0353	———	

(a_1),(a_2),(b) All conditions as in Tables (4) and (5).

TABLE (6). Total forward movement of the aerodynamic centre due to the influence of the body.

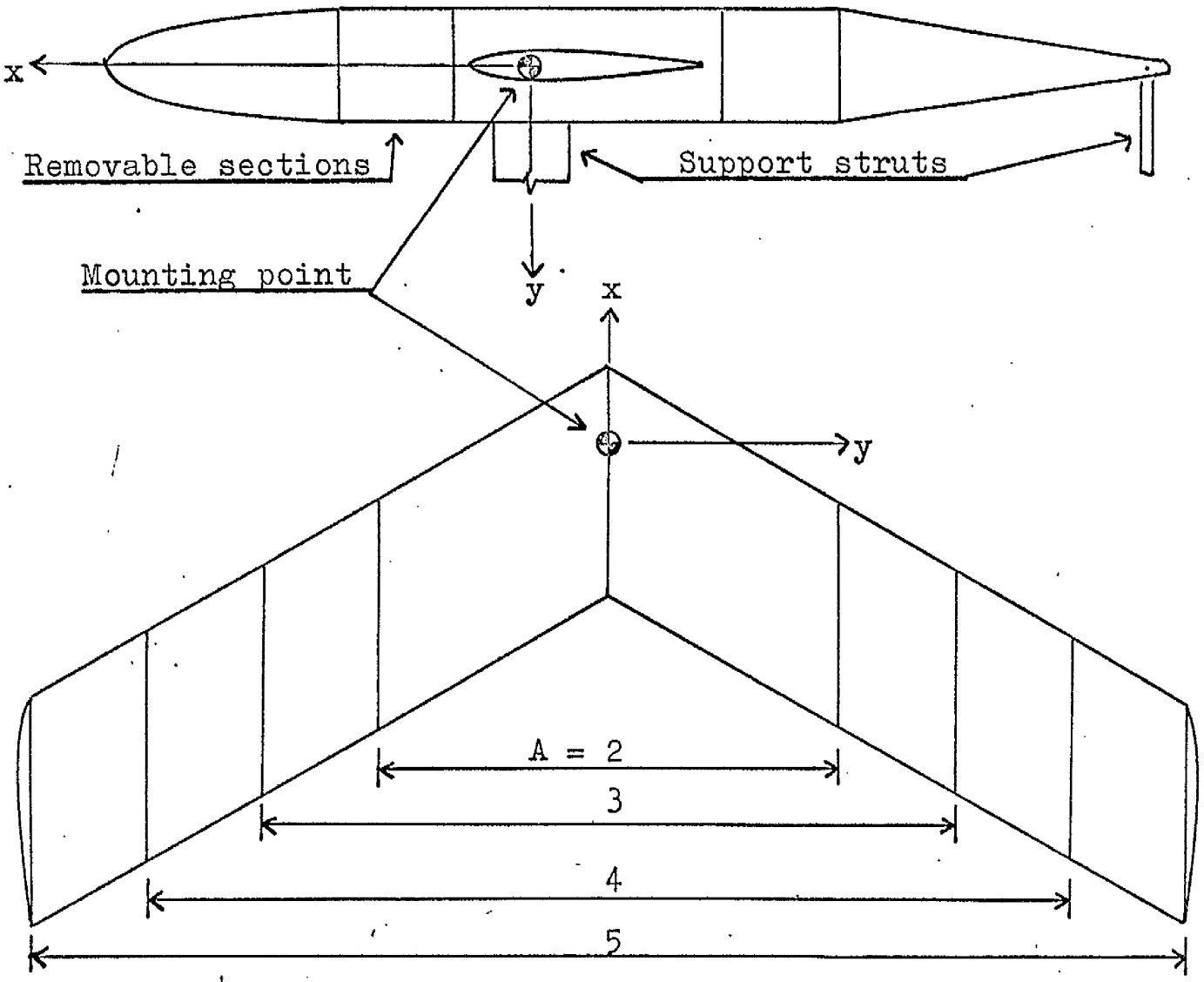

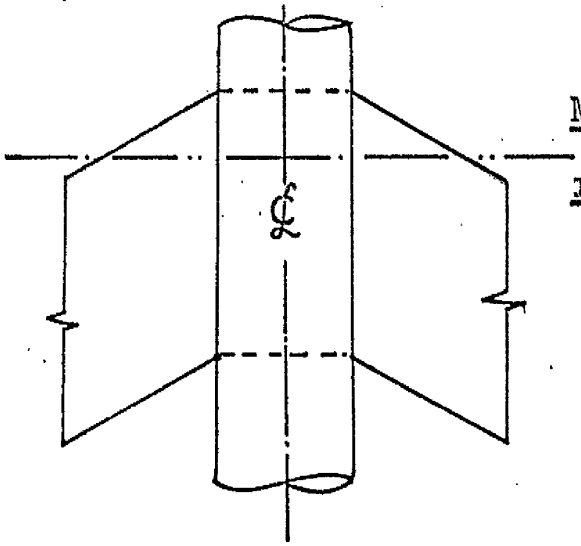

Mounting at root $\frac{c}{4}$.

3 – bolts per joint

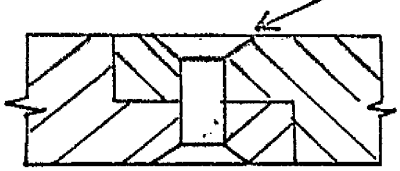

Enlarged view of typical joint.

FIG. (1). Typical wing and wing/body combination.

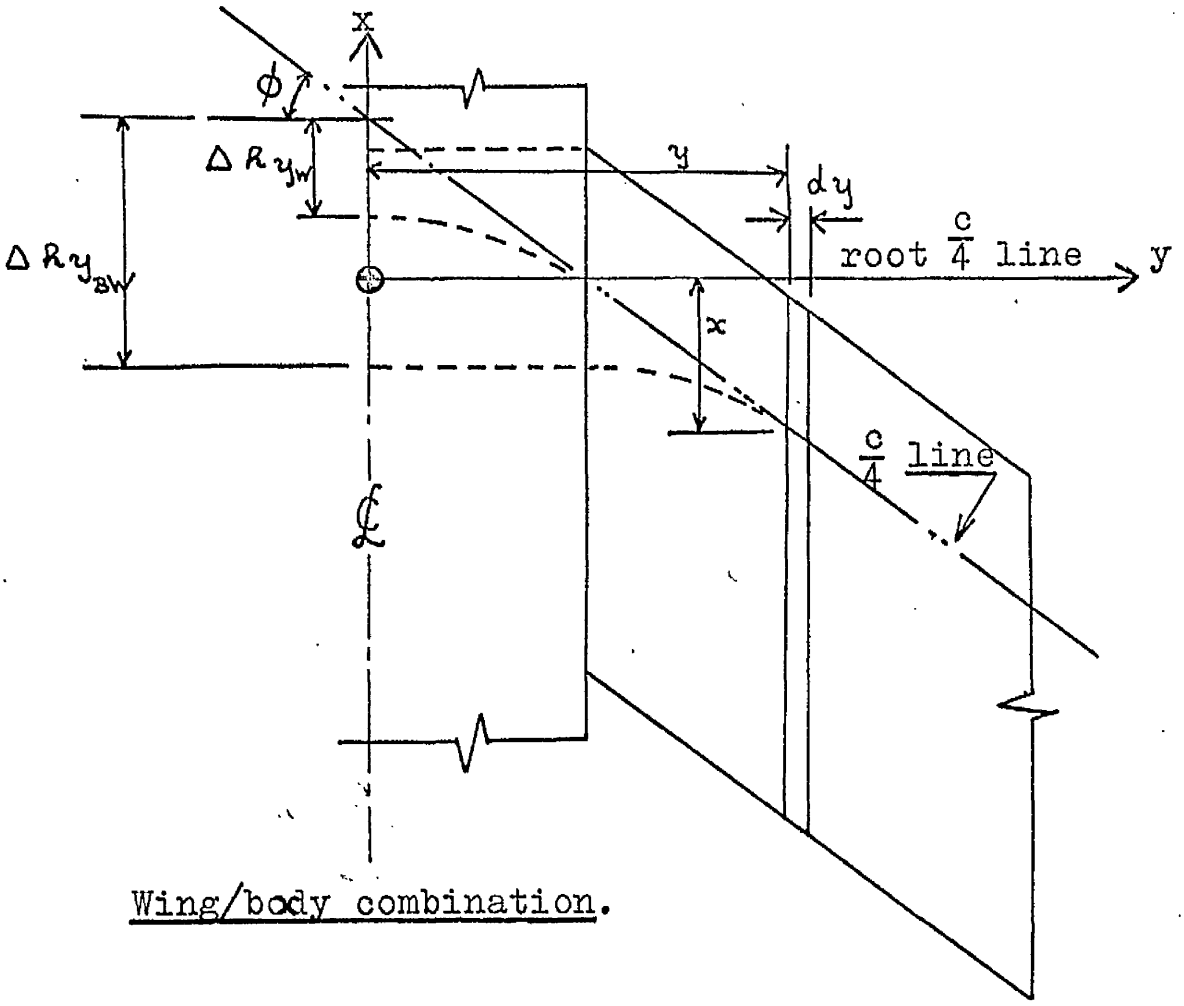

Wing/body combination.

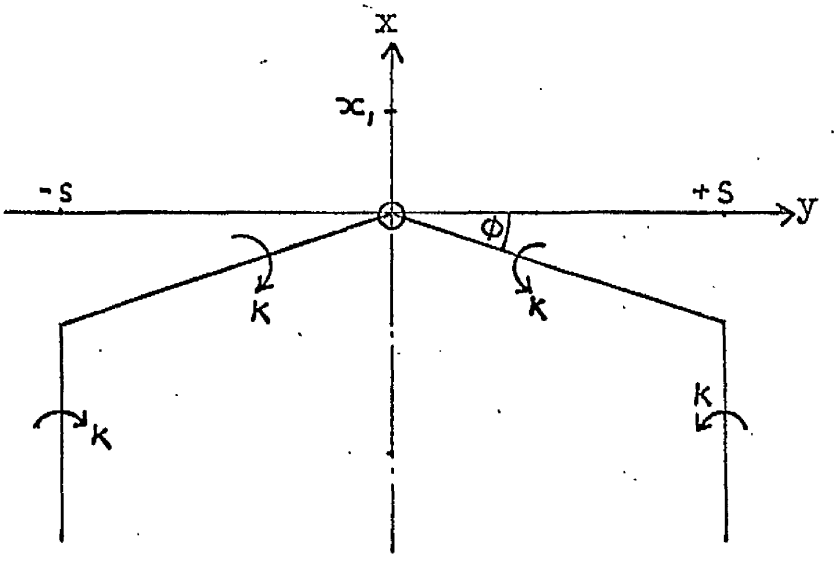

Sweptback horse-shoe vortex.

FIG. (1). (cont.)

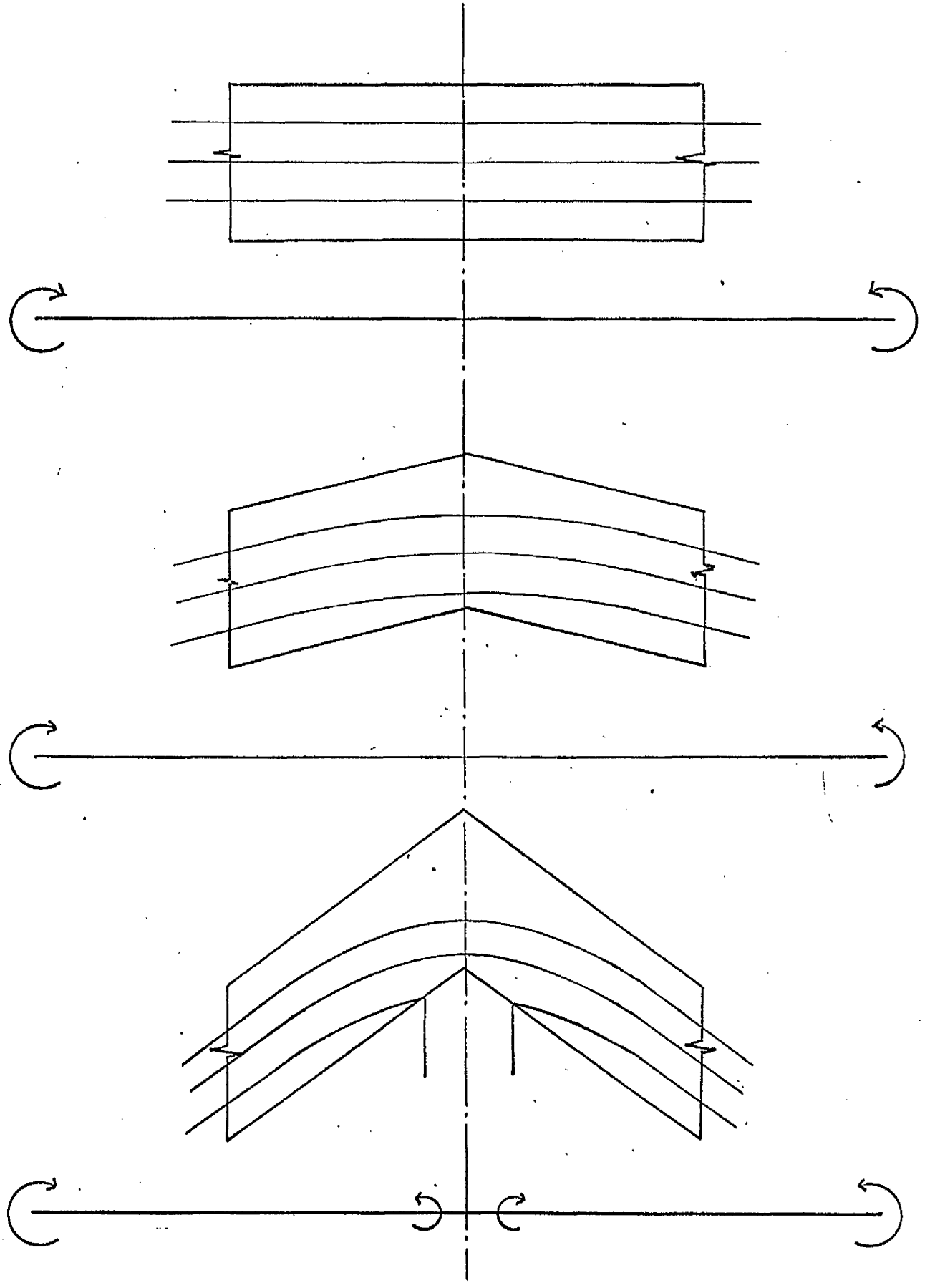

FIG. (1). (concl.)

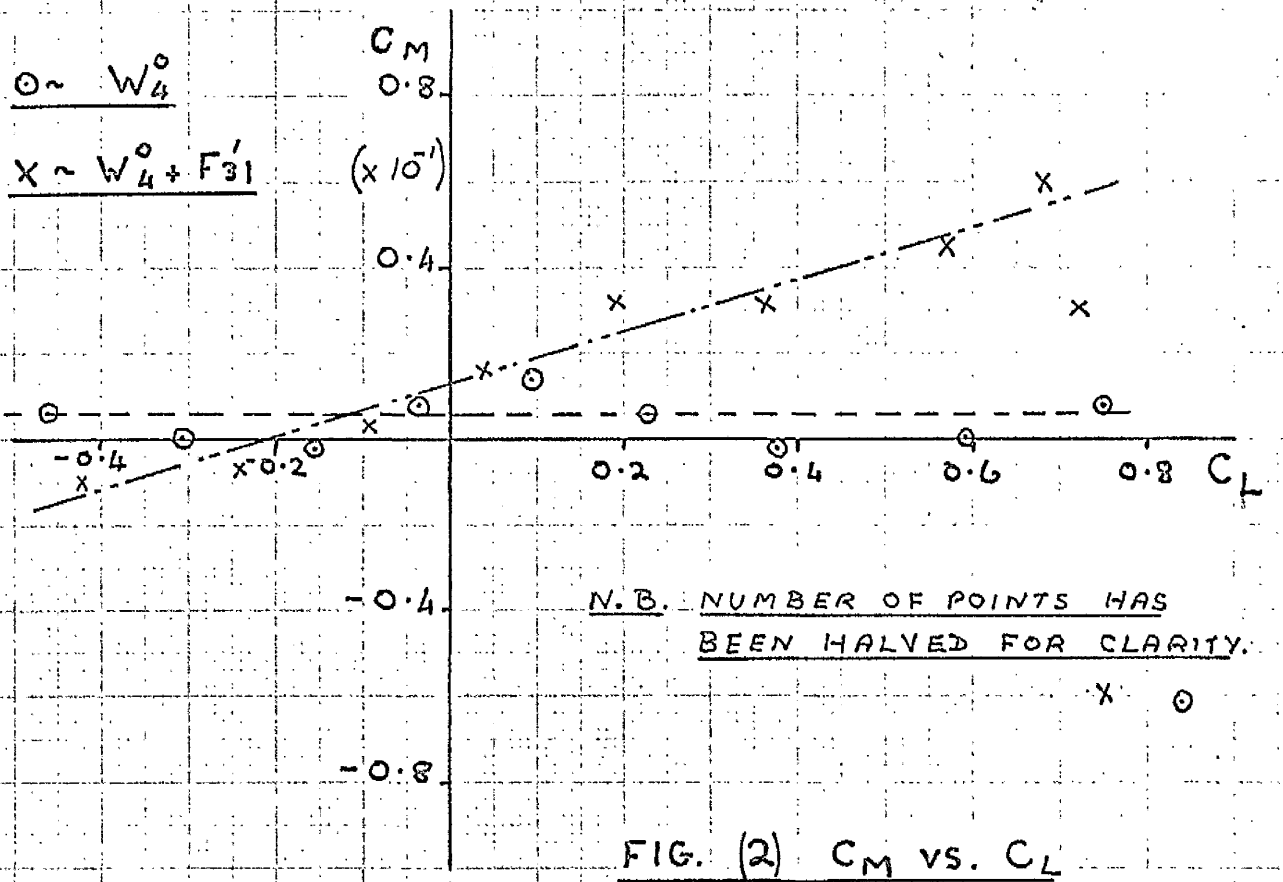

N.B. NUMBER OF POINTS HAS BEEN HALVED FOR CLARITY.

FIG. (2) C_M VS. C_L

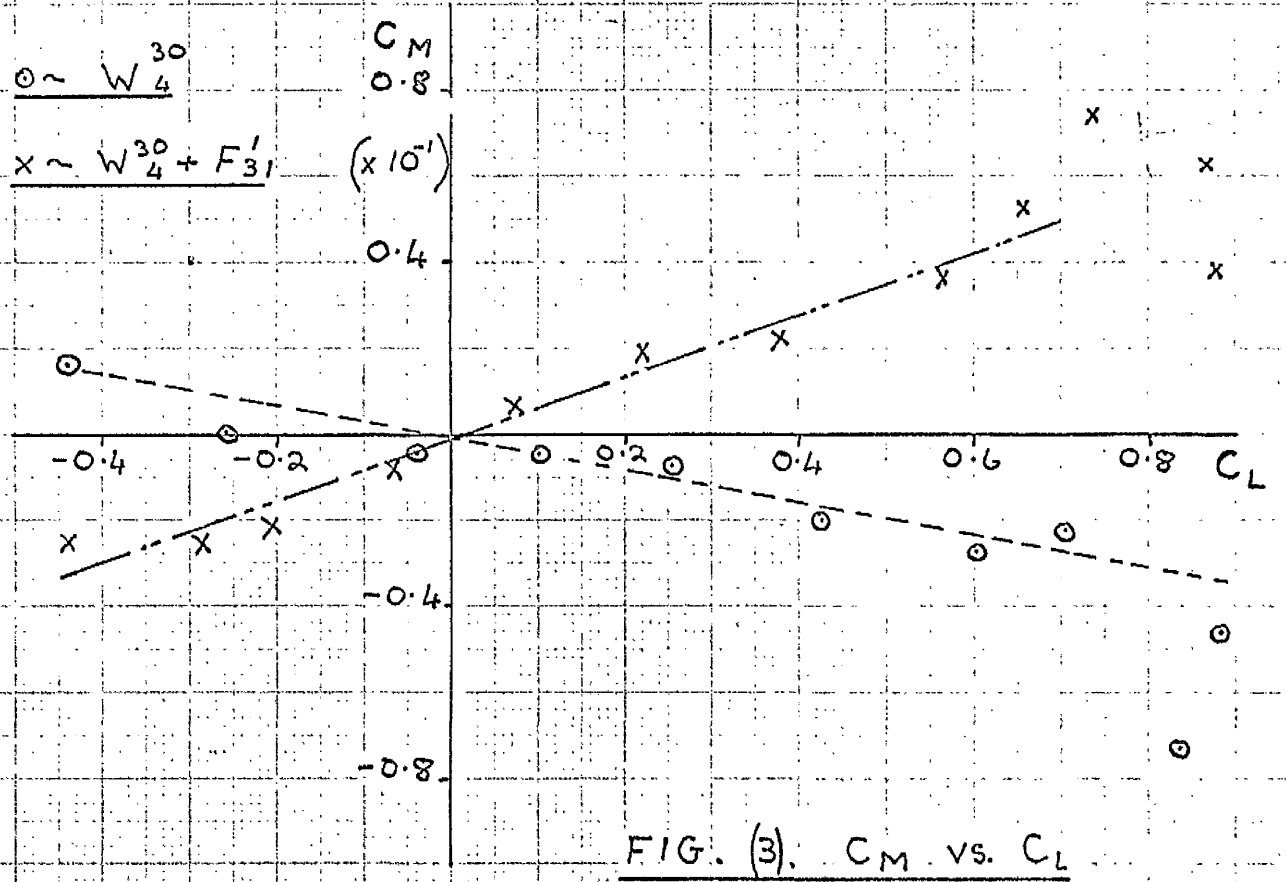

FIG. (3). C_M VS. C_L

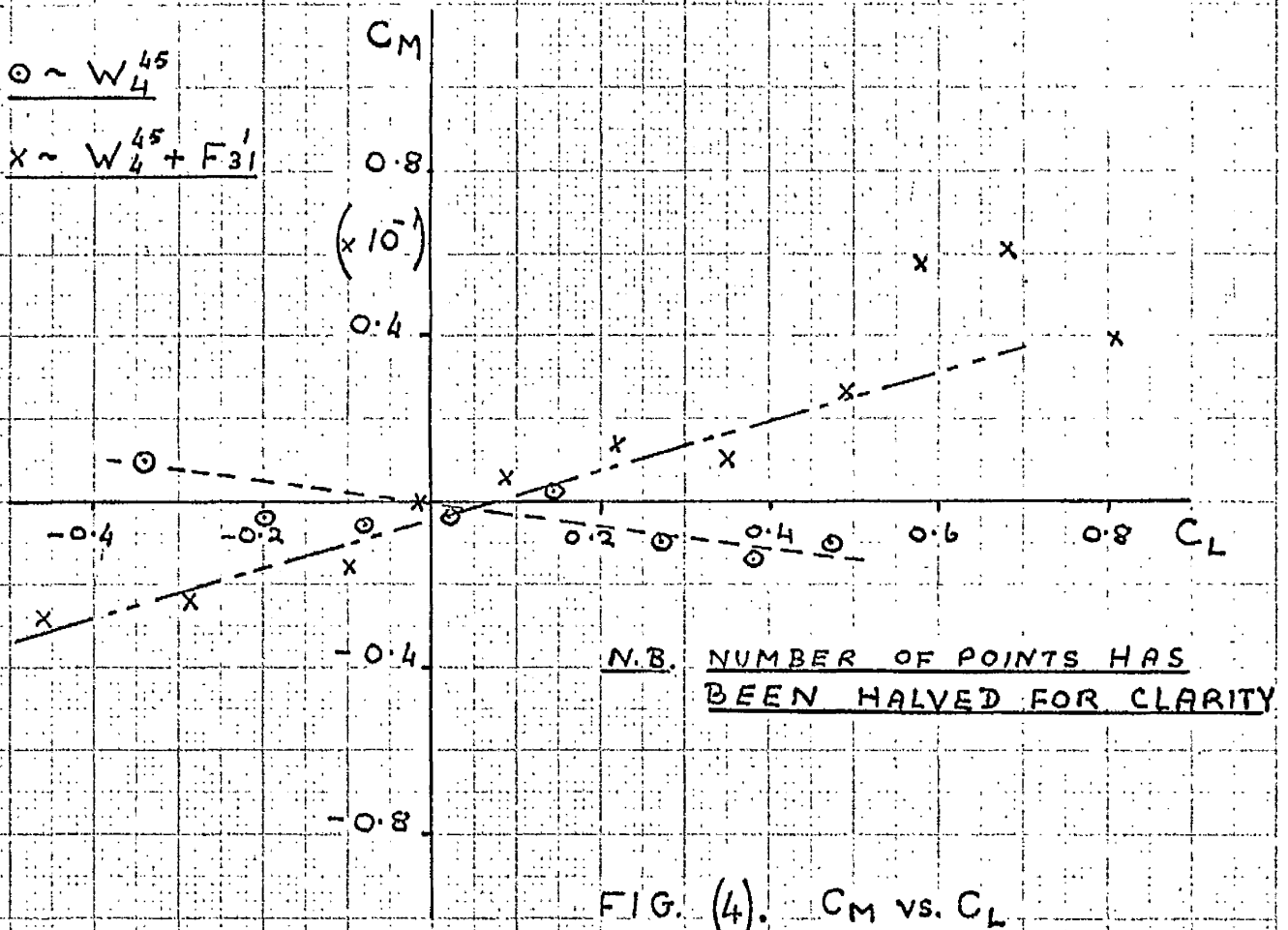

N.B. NUMBER OF POINTS HAS BEEN HALVED FOR CLARITY

FIG. (4). C_M vs. C_L

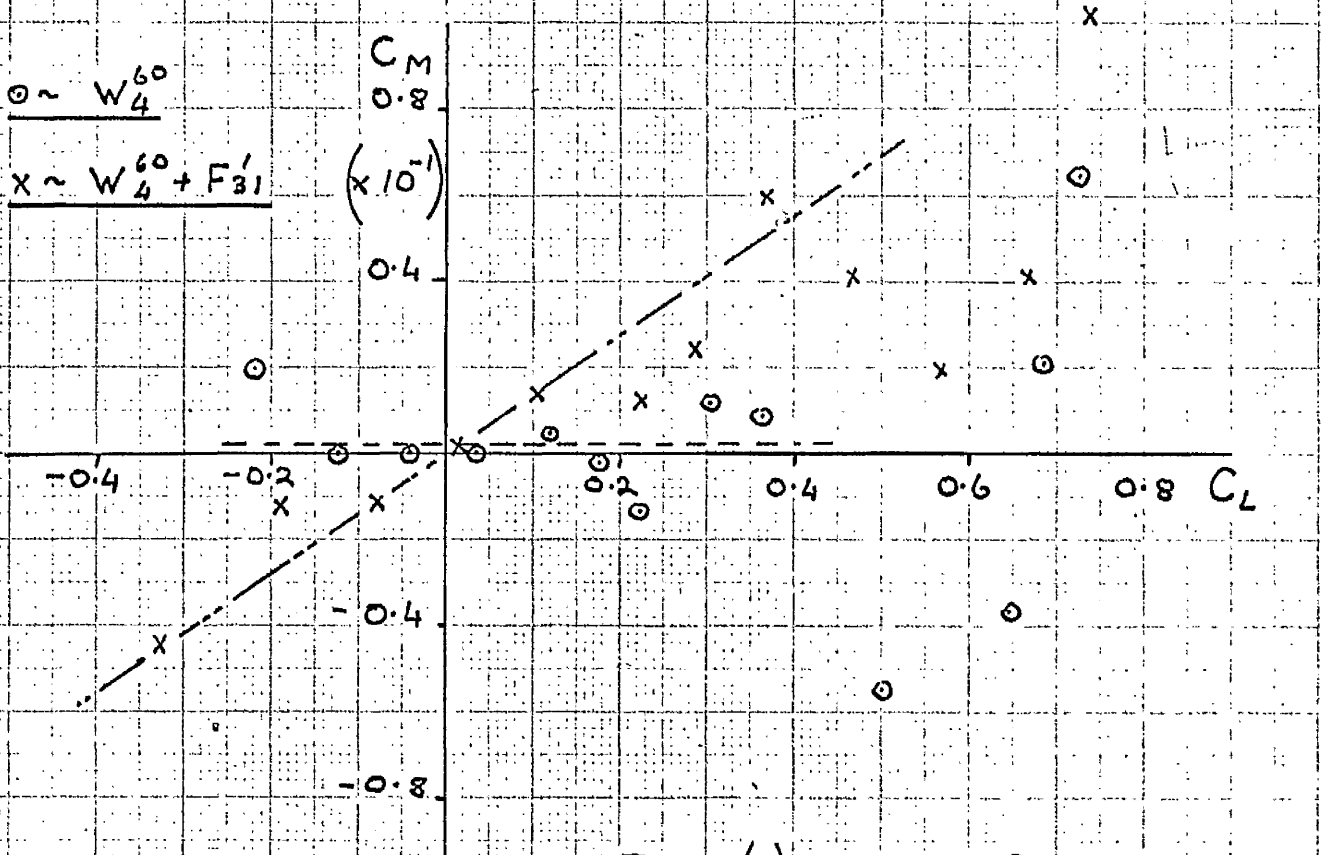

FIG. (5). C_M vs. C_L.

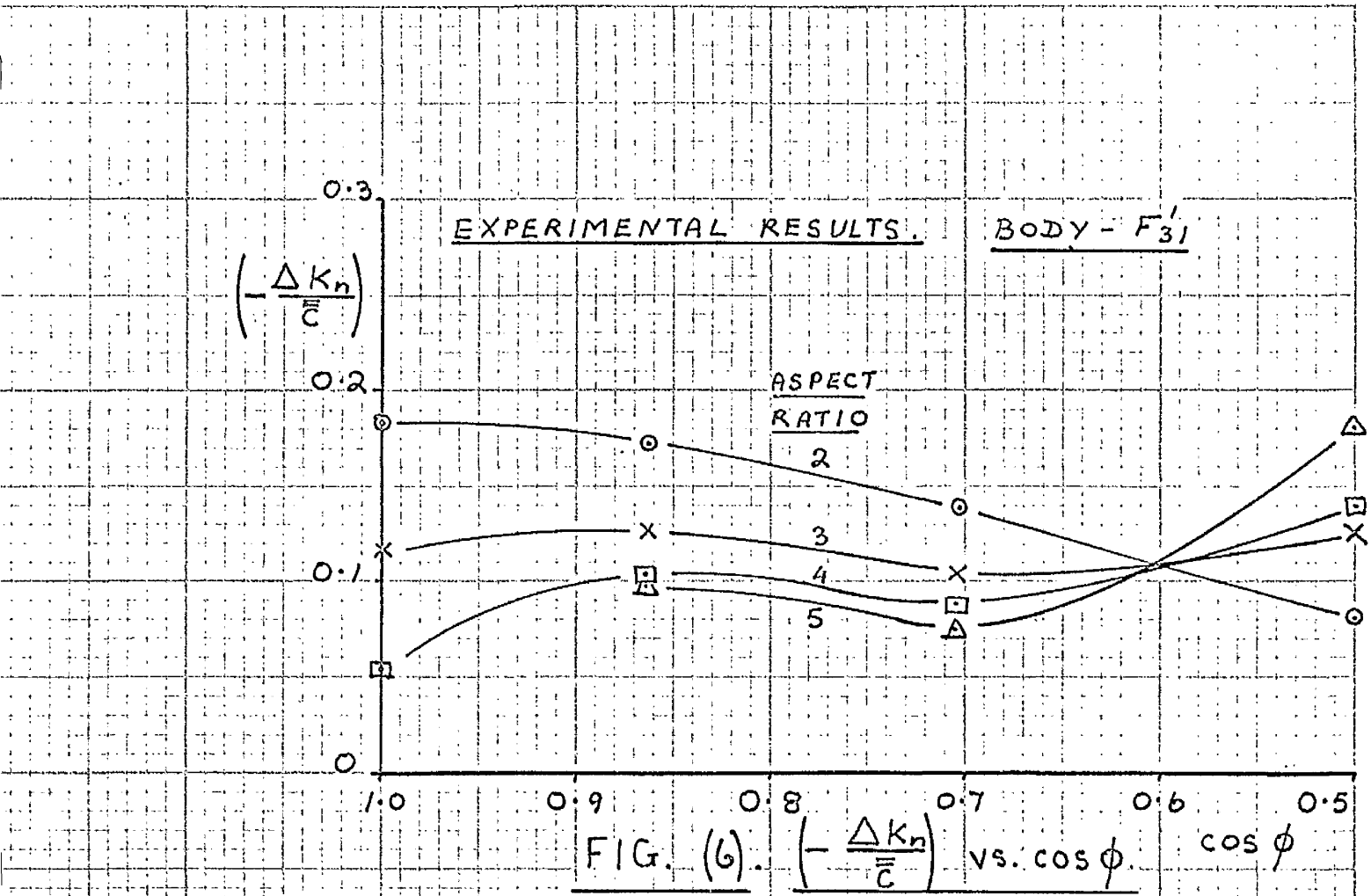

FIG. (6). $\left(-\frac{\Delta K_n}{\bar{C}}\right)$ vs. cos φ

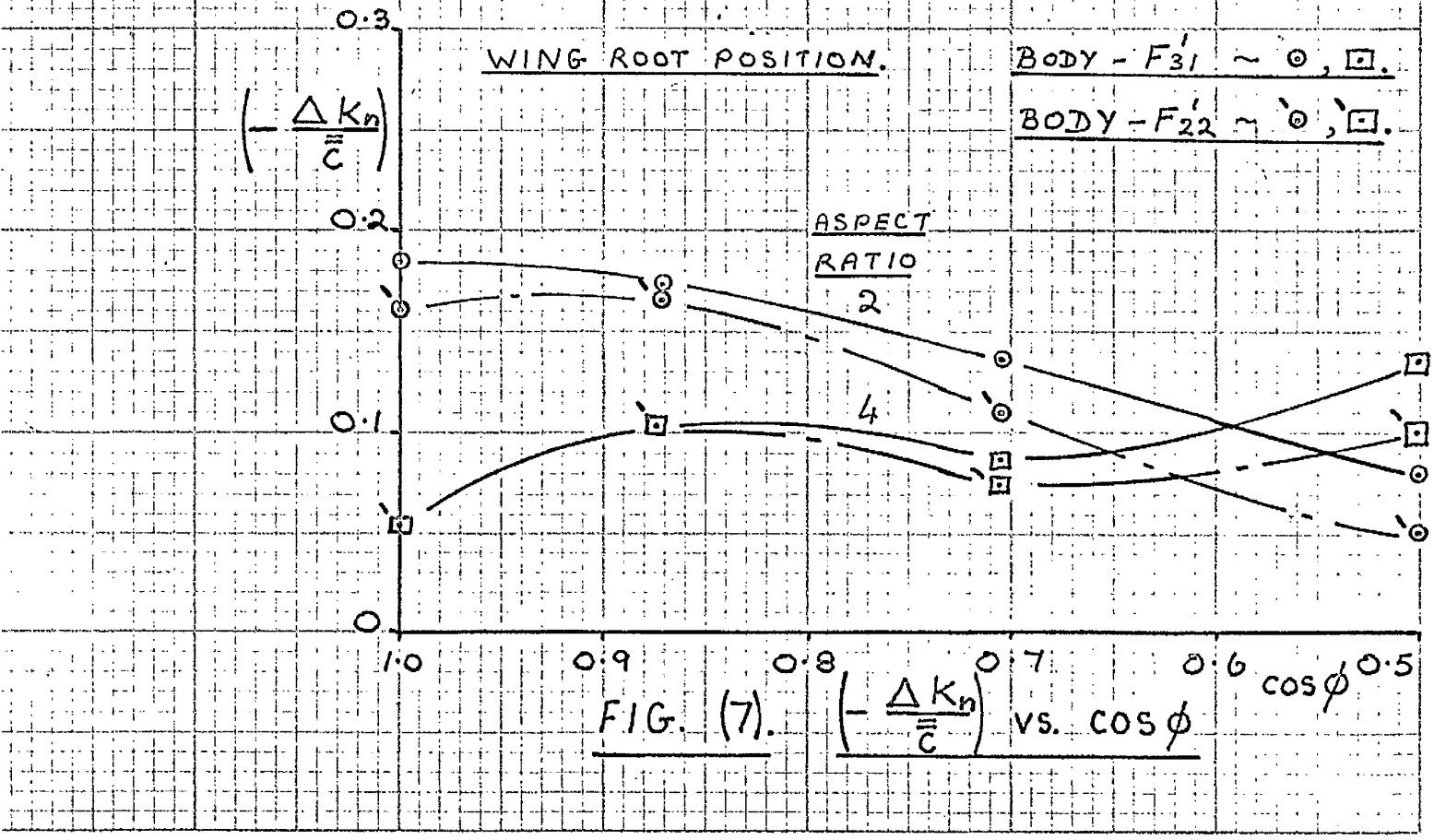

FIG. (7). $\left(-\frac{\Delta K_n}{\bar{C}}\right)$ vs. cos φ

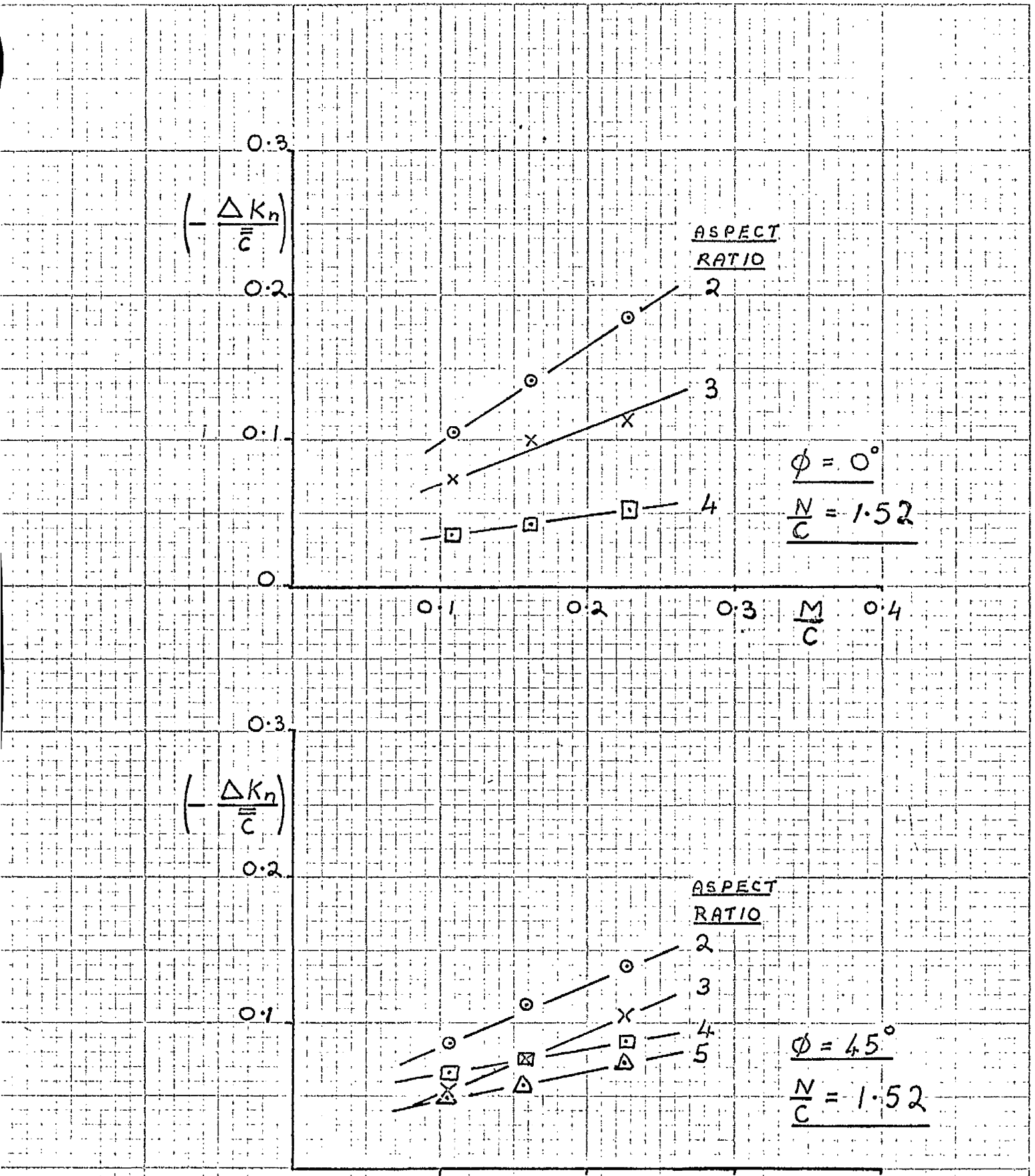

FIG. (8) $\left(-\frac{\Delta K_n}{\bar{C}}\right)$ VS. $\frac{M}{C}$

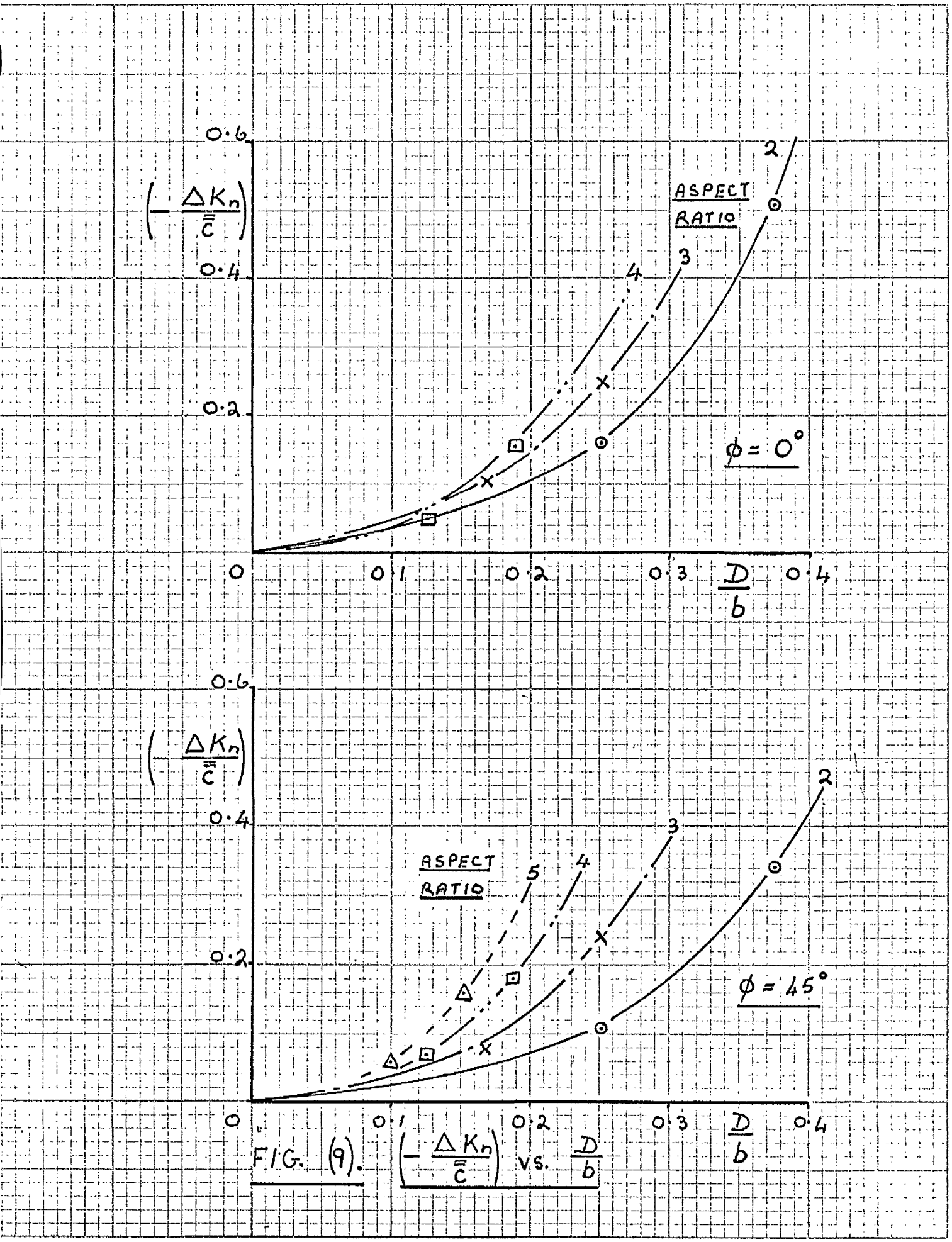

FIG. (9). $\left(-\frac{\Delta K_n}{\bar{c}}\right)$ vs. $\frac{D}{b}$

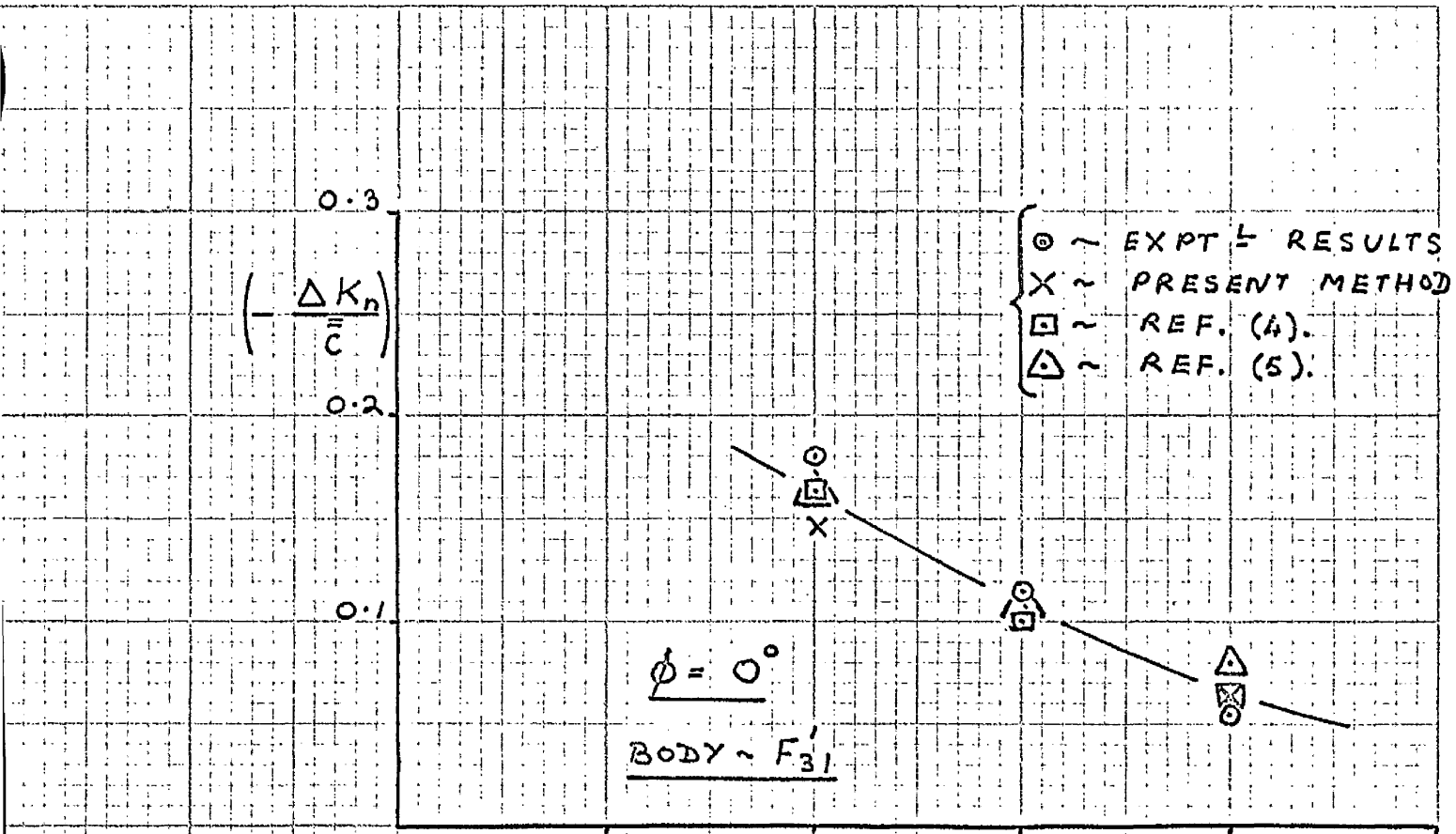

FIG. (10). $\left(-\frac{\Delta K_n}{\bar{C}}\right)$ Vs. ASPECT RATIO.

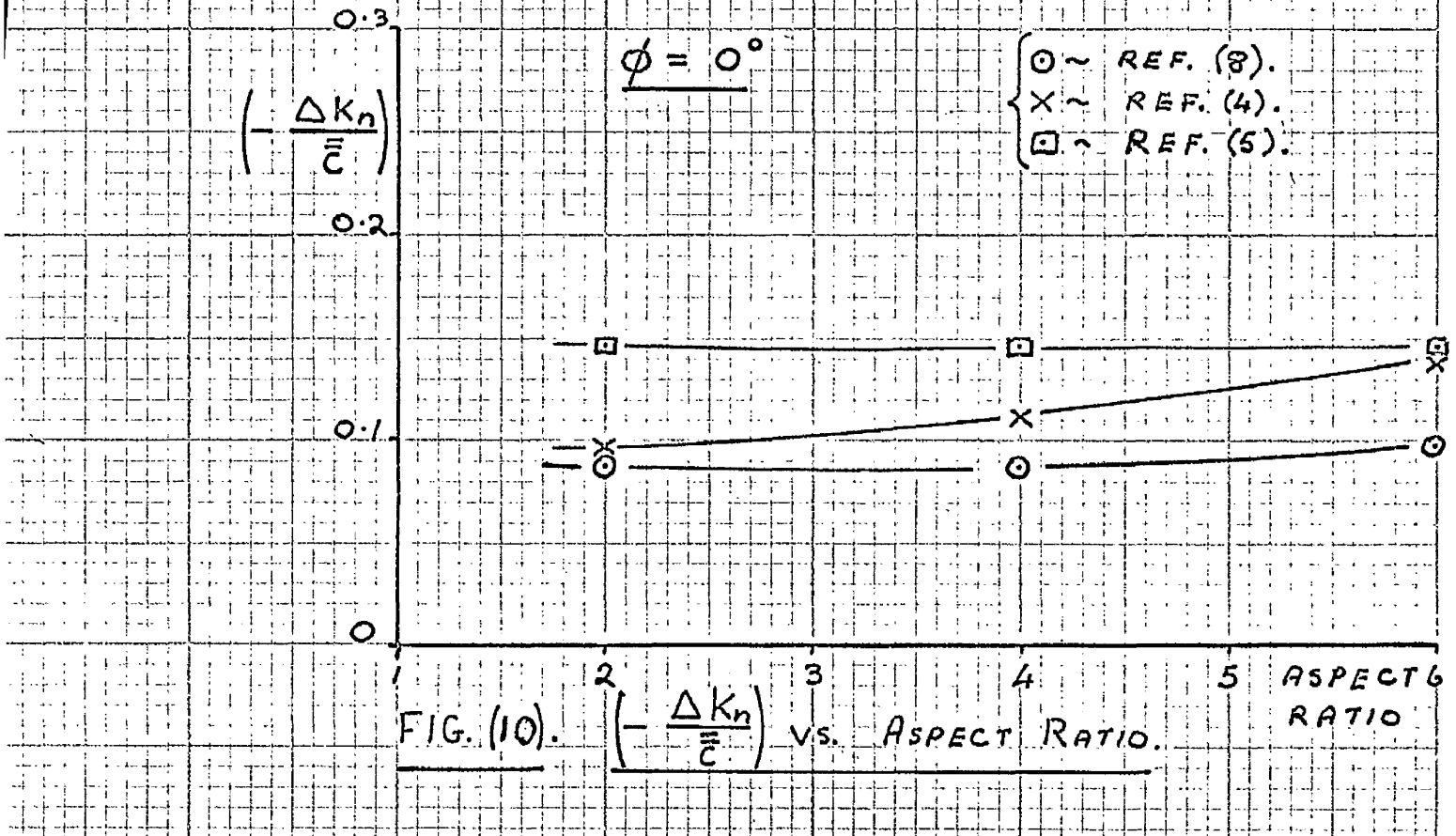

FIG. (10). $\left(-\frac{\Delta K_n}{\bar{C}}\right)$ Vs. ASPECT RATIO.

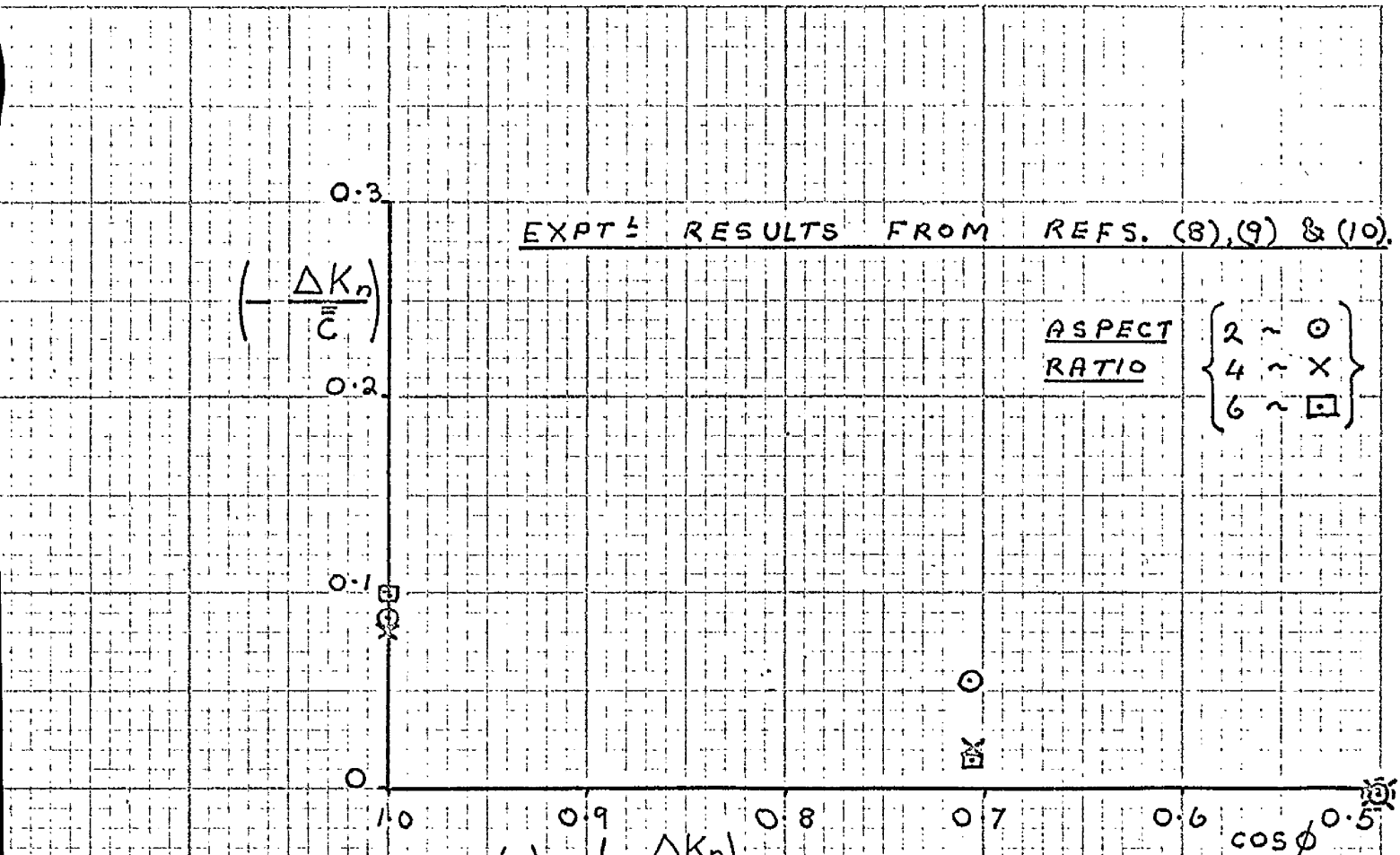

FIG. (11) $\left(-\frac{\Delta K_n}{\bar{C}}\right)$ Vs. cos ϕ

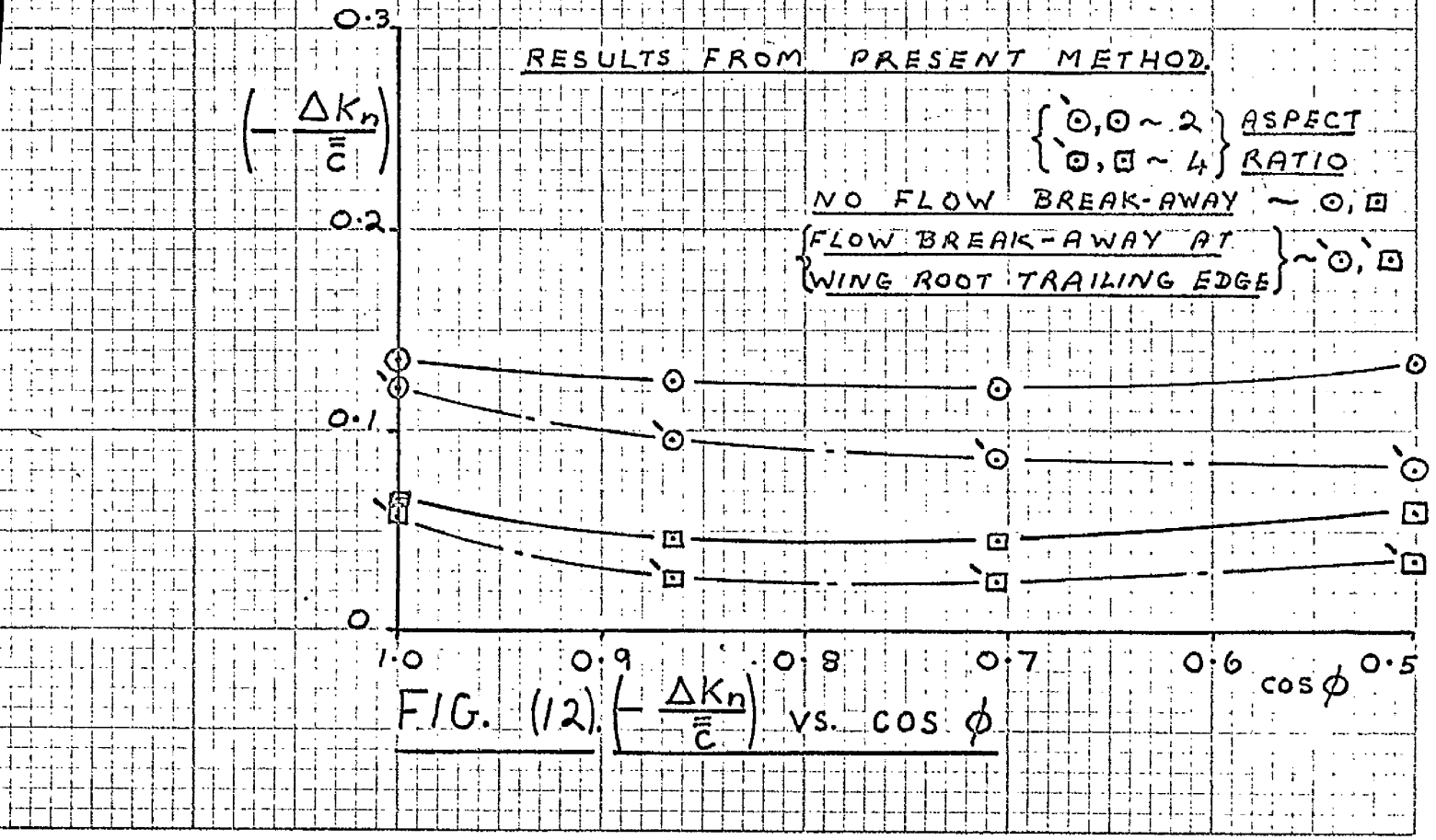

FIG. (12) $\left(-\frac{\Delta K_n}{\bar{C}}\right)$ vs. cos ϕ

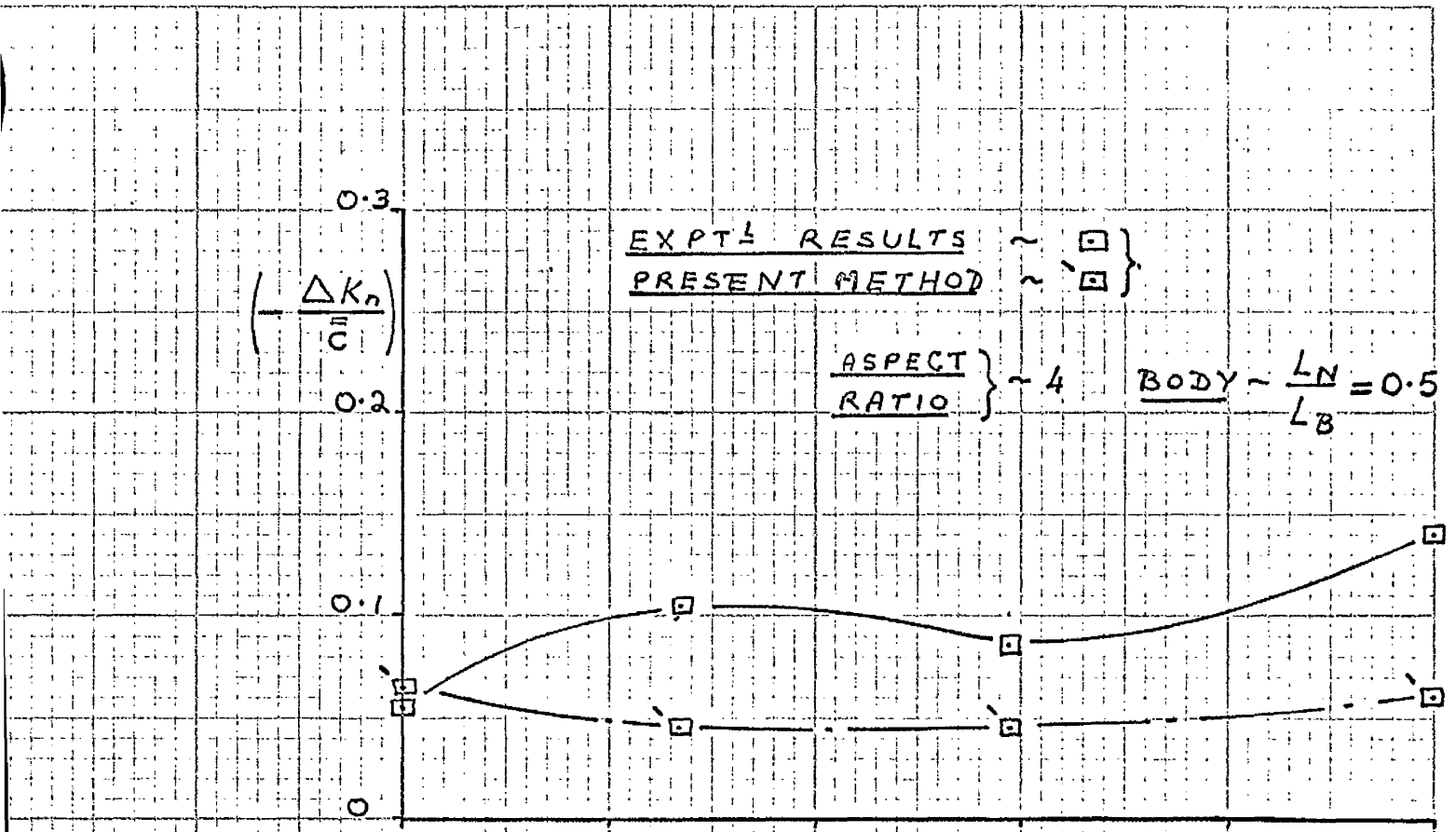

FIG. (15). $\left(-\frac{\Delta K_n}{\bar{C}}\right)$ vs. cos ϕ.

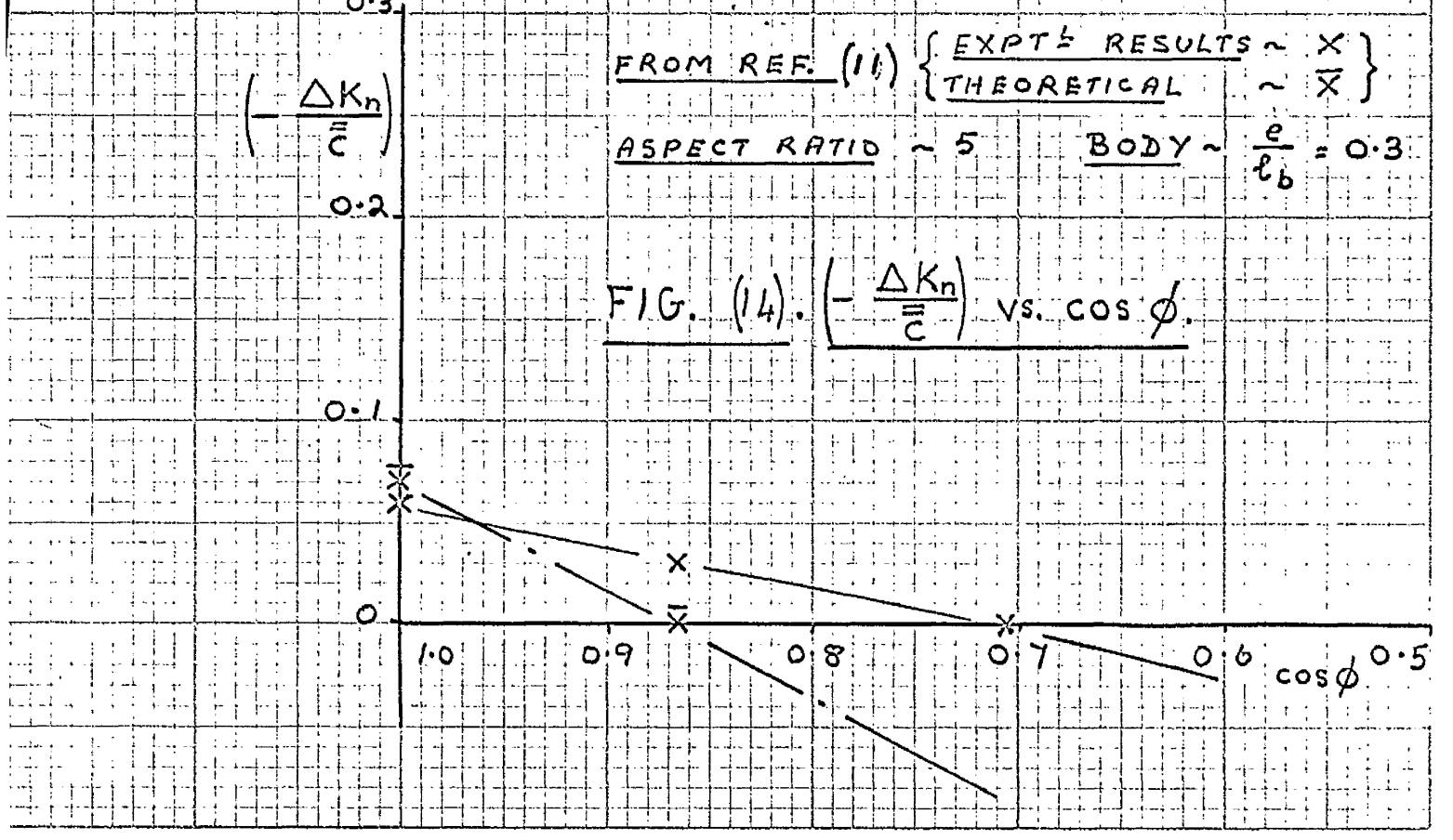

FIG. (14). $\left(-\frac{\Delta K_n}{\bar{C}}\right)$ vs. cos ϕ.

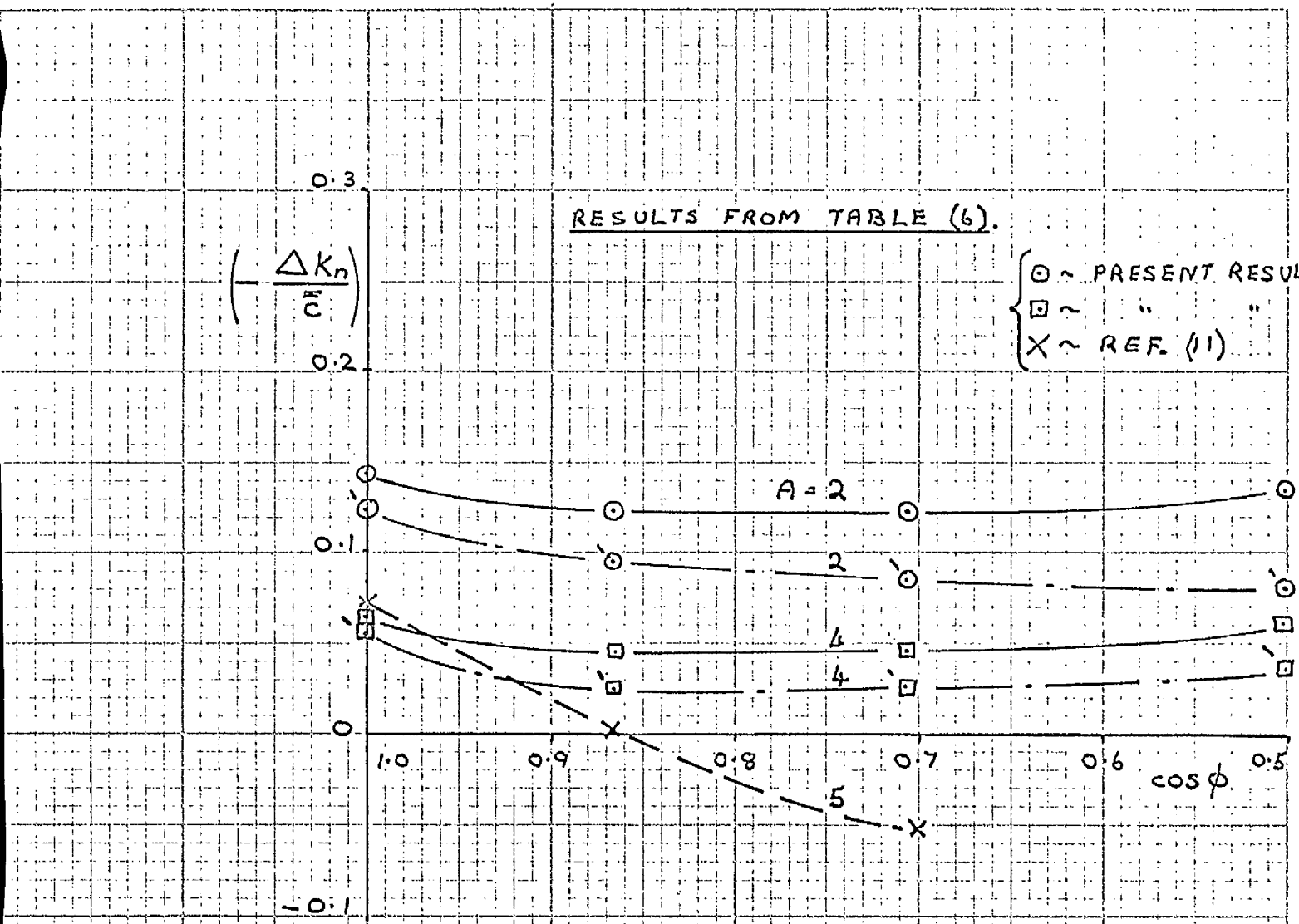

FIG. (16). $\left(-\frac{\Delta K_n}{\bar{\bar{c}}}\right)$ vs. $\cos\phi$

DOWNWASH DISTRIBUTIONS IN THE REGION OF A HORSE-SHOE VORTEX

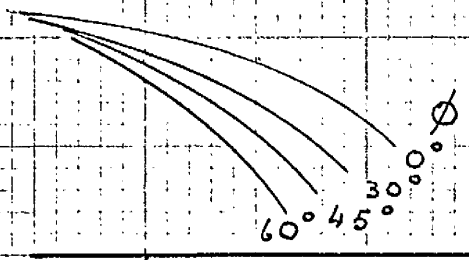

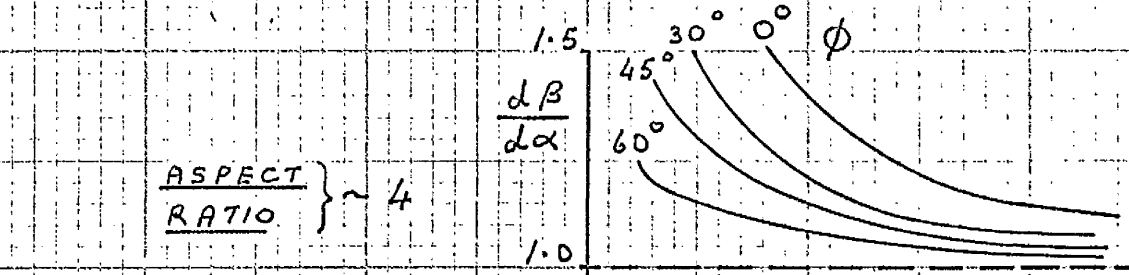

ASPECT RATIO } ~ 4

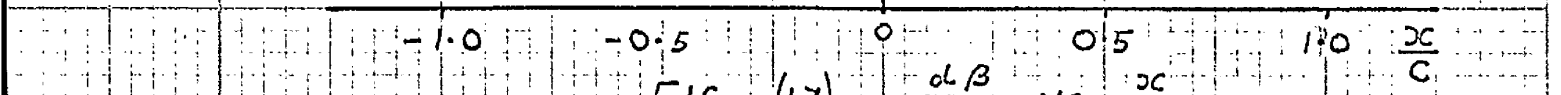

FIG. (17). dβ/dα VS. x/c

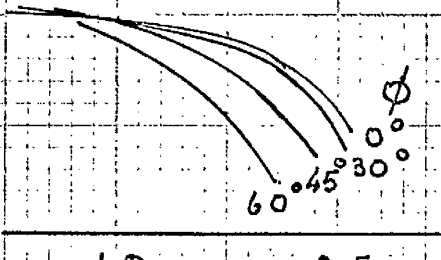

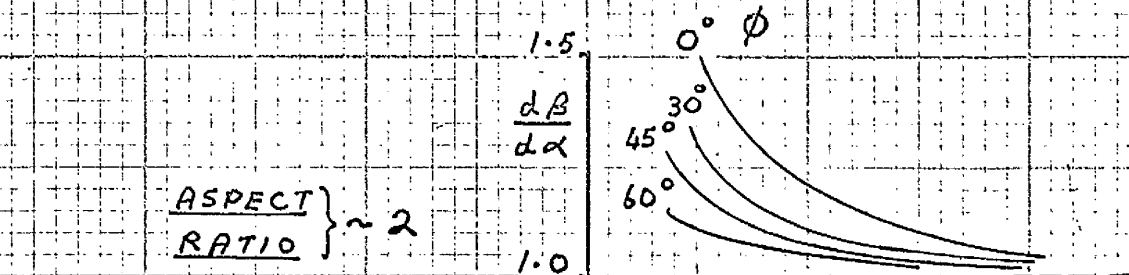

ASPECT RATIO } ~ 2

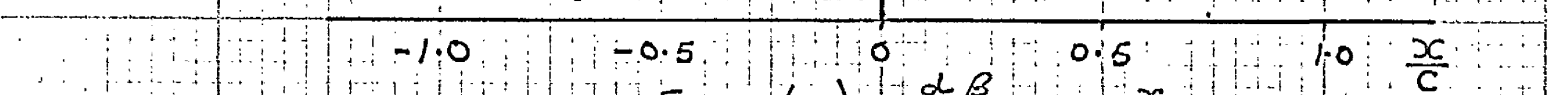

FIG. (18). dβ/dα VS. x/c

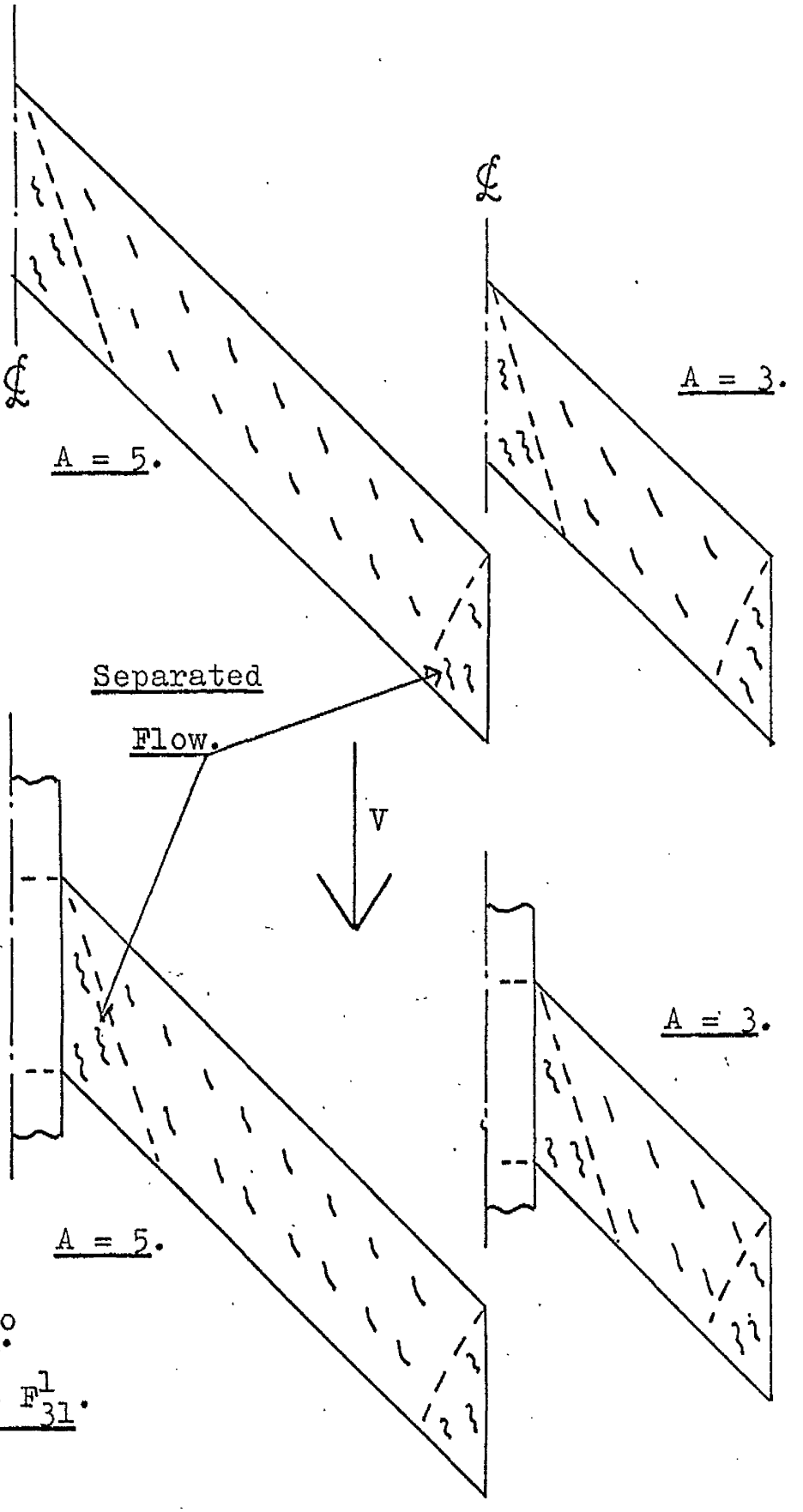

FIG. (19). Tuft tests. Diagrammatic sketchs showing the flow on the wings and wings/body combinations.

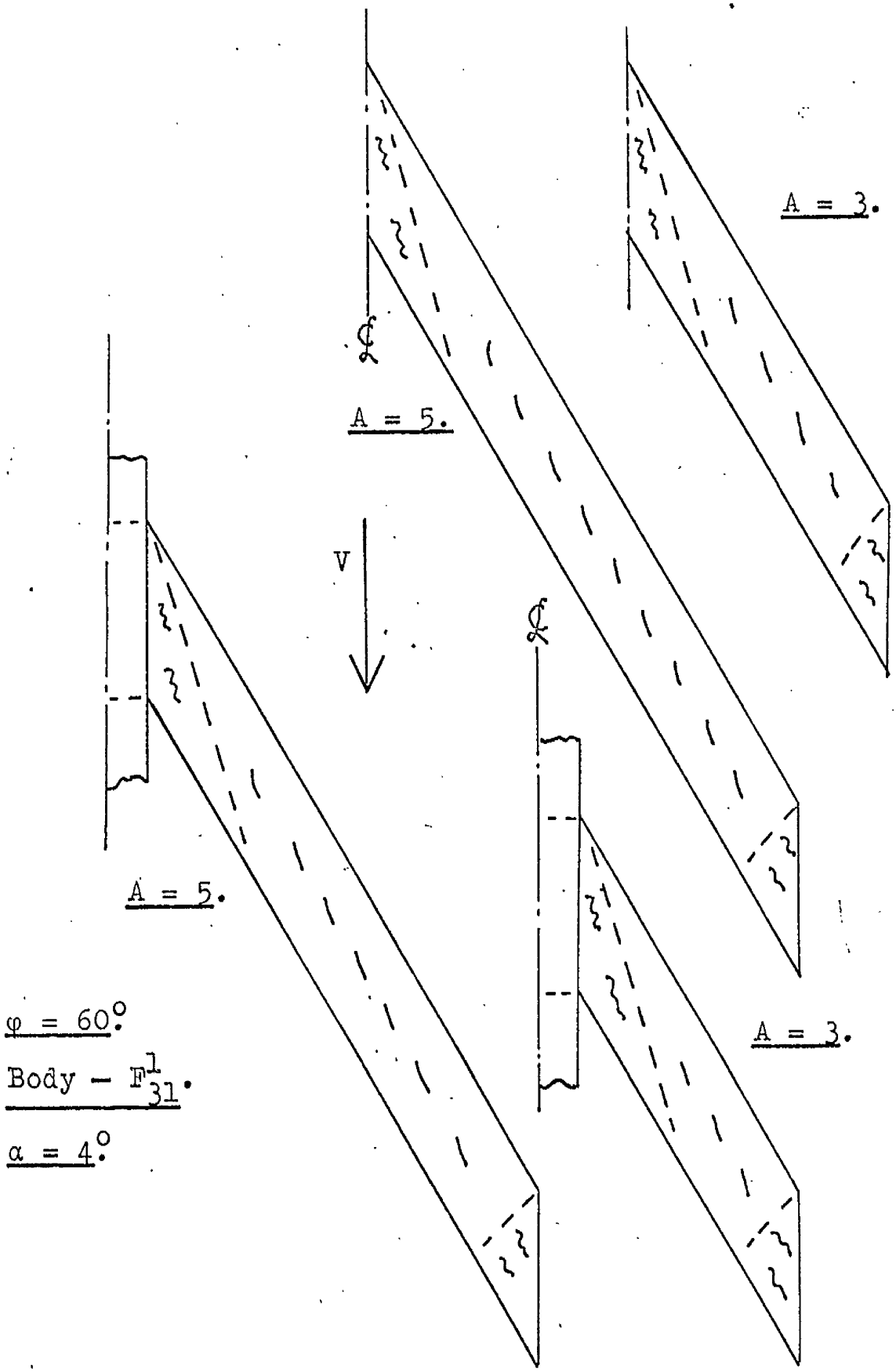

FIG. (19). Tuft tests. Diagrammatic sketchs of the flow on the wings.

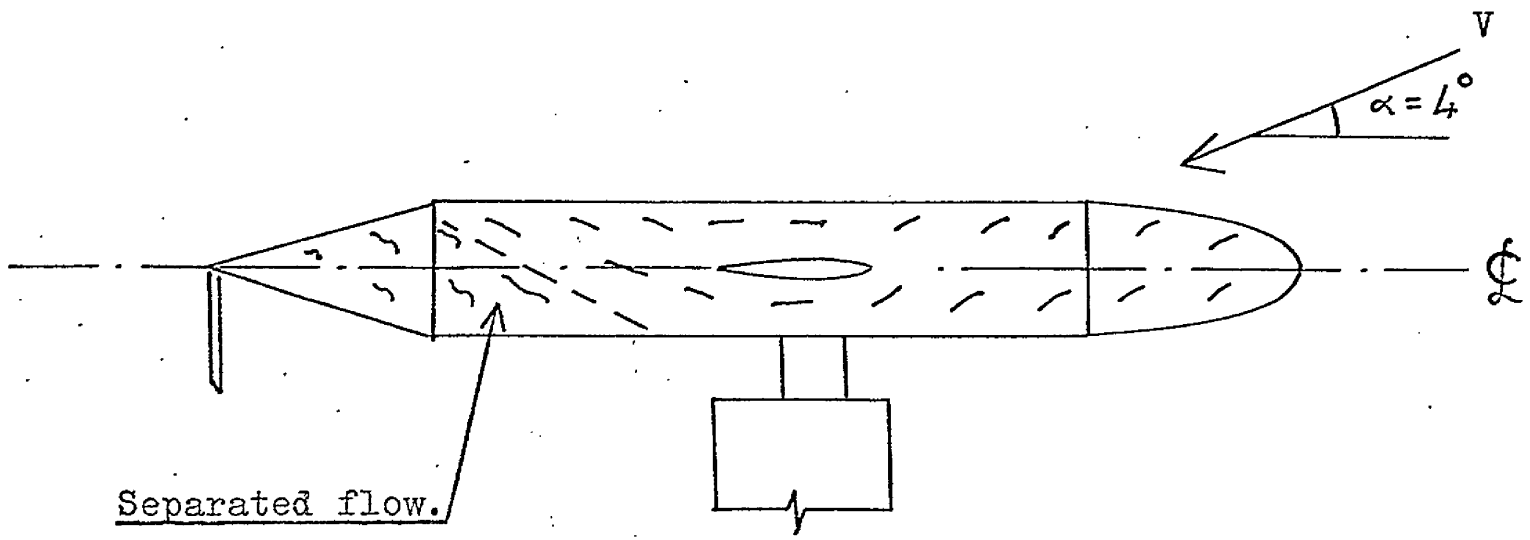

FIG.(20). Tuft tests. Diagrammatic sketch showing flow on the body.